NUCLEAR ENGINEERING EDUCTION RESEARCH (NEER)
ANNUAL PROGRESS REPORT

Project Title:

SURFACE MODIFICATION OF FUEL CLADDING MATERIALS WITH INTEGRAL FUEL BURNABLE ABSORBER BORON

Grant No.: DE-FG07-O5ID14708

Annual Report
July 1st 2005 to June 30th 2008

Submitted by:

Lead Organization:

University of Wisconsin, Madison
Dr. Kumar Sridharan
Dr. Todd Allen
Mr. Jesse Gudmundson (student, nuclear engineering)
Mr. Benjamin Maier (student, materials science and engineering)

Collaborating Organizations:

Sandia National Laboratories, Albuquerque, NM
Collaborator: Dr. Timothy Renk

Westinghouse Electric Company - Science and Technology Department, Pittsburgh, PA
Collaborators: Dr. Edward Lahoda and Dr. Warren Junker

Submitted on: November 3, 2008

TABLE OF CONTENTS

PROJECT OBJECTIVES AND SUMMARY

Integral fuel burnable absorbers (IFBA) are added to some rods in the fuel assembly to counteract excessive reactivity. These IFBA elements (usually boron or gadolinium) are presently incorporated in the UO_2 pellets either by mixing in the pellets or as coatings on the pellet surface. In either case, the incorporation of IFBA into the fuel has to be performed in a nuclear-regulated facility that is physically separated from the main plant. These operations tend to be costly and can add from 20 to 30% to the manufacturing cost of the fuel. Other cost and performance issues concerning the addition of IFBA elements in the fuel pellets are the reduction in fuel melting point, parasitic neutron absorption at fuel's end-of-life, build-up of pressure inside the cladding due to generation of transmutation gases, and expensive end-of-life separation operations. These issues are likely to be exacerbated in the next generation of nuclear reactors which will likely use long-lived fuels with higher enrichments of ^{235}U or other fissile materials to permit fuel loadings that last anywhere from 4 to 8 years.

The goal of this NEER research project was to develop an alternative approach that involves incorporation of IFBA element boron at the surface of the fuel cladding material. The anticipated long-term practical goal of this research is to be able to introduce boron in the outer surface of the fuel cladding rather than as an additive to the fuel pellets. This alternative approach will allow for the introduction of the IFBA in a non-nuclear regulated environment and will obviate the necessity of additional handling and processing of the fuel pellets. This could represent significant cost savings and potentially lead to greater reproducibility and control of the burnable fuel in the early stages of the reactor operation. The project was a collaboration between University of Wisconsin, Sandia National Laboratories, and Westinghouse Corporation.

The incorporation of boron into the surface of cladding materials was performed using two novel approaches: (i) the IBEST (Ion Beam Surface Treatment) process developed at Sandia National Laboratories, that involves the near-surface melting by the delivery of energetic ion beam pulses onto the surface of a material to achieve surface alloying and (ii) SIMAT (Supersonically Induced Mechanical Alloy Technology), a cold spray process under development at Westinghouse to deposit an adherent coating of zirconium diboride on the surface of the cladding material. A fundamental difference between the two processes is that IBEST is a surface alloying process, whereas the SIMAT process results in an overlay coating. All basic materials research and characterization work of the untreated and surface treated samples were performed at the University of Wisconsin.

To provide broad-based relevance of this research concept to a variety of future nuclear reactors, three candidate fuel cladding materials are being investigated as substrates in this research: (i) Zirlo (a widely used HCP zirconium alloy developed by Westinghouse), (ii) NF616, a BCC ferritic-martensitic steel, and (iii) FCC 316 austenitic stainless steel. To evaluate the thermal stability of the modified surfaces in a prototypic reactor environment, the samples were tested in both high temperature steam and supercritical water environments. Supercritical water tests were performed at the University of Wisconsin and high temperature steam autoclave tests were performed at Westinghouse. All materials characterization after high temperature testing was performed at the University of Wisconsin. A modeling effort was initiated to complement the IBEST surface treatment being performed at Sandia National Laboratories. Here, 1-D mixing dynamics simulations were used to predict the melt depth and melt duration of the boron sputtered, IBEST-treated samples. The radiation stabilities of the IBEST and cold-spray treated Zirlo alloys are presently being tested at the Idaho National Laboratory.

Our previous studies (prior to this NEER project) showed that another IFBA element gadolinium could be successfully alloyed into Zirlo alloy using Sandia's IBEST process. However, steam autoclave testing of these samples at Westinghouse showed that the Gd-alloyed Zirlo samples exhibited 2 to 3 times greater weight gain due to oxidation as compared to the control Zirlo samples. To arrive at a solution to this problem we have investigated a multi-layer approach wherein a top layer of pure zirconium is applied above the Gd-alloyed Zirlo layer, as a part of this NEER project. This approach in effect provides for a sub-surface Gd-containing layer which is shielded from the environment by the outer corrosion resistant zirconium layer. Three approaches to achieving this multi-functional, multi-layered surface have been investigated. This task was added [and reported to DoE at the end of year 1 of this NEER project] because it brings considerable value to the overall objectives of this NEER project of incorporating IFBA elements in the outer surfaces of fuel cladding.

SUMMARY OF RESEARCH ACCOMPLISHMENTS IN THIS NEER PROJECT

The following are the specific research accomplishments of this NEER program:

1. Incorporation of IFBA boron at the surface of three potential fuel cladding materials, NF616 ferritic steel, Zirlo, and 316 stainless steel followed by high temperature testing in steam autoclave (427^{o}C, 100 atmospheres) and supercritical water (500^{o}C, 3600psi) to evaluate the oxidation resistance of modified surfaces.
2. Development of three experimental IBEST approaches aimed at achieving multi-functional, multi-layered surfaces in which a sub-surface gadolinium IFBA layer is shielded by an outer corrosion resistant Zr layer followed by testing of samples in steam autoclaves at Westinghouse.
3. Development of IBEST process to alloy a pre-sputtered boron layer (1 to 1.5μm thick) using the IBEST process.
4. Development of 1-D liquid phase mixing models to predict the depth of the surface modified layers in the IBEST process
5. Deposition of 1 to 2μm thick zirconium-diboride coating on the three alloy substrates using a cold spray process developed at Westinghouse.
6. Characterization of IBEST surface treated samples.
7. Characterization of cold sprayed samples.
8. Supercritical water (SCW) corrosion testing of IBEST and cold sprayed samples.
9. Characterization of IBEST and cold sprayed samples after supercritical water testing.
10. High temperature steam autoclave testing of IBEST and cold sprayed samples.
11. Characterization of IBEST and cold sprayed samples after high temperature steam autoclave testing.
12. Weight change measurements after high temperature corrosion tests to quantify corrosion resistance.
13. Radiation testing at Idaho National Laboratory (ongoing)
14. Presentation of the work by student Mr. Jesse Gudmundson at the University of Wisconsin, Undergraduate Research Symposium held in April 2007 and at the DoE-NEER sponsored technical session at the American Nuclear Society Annual Conference in Boston in June 2007. Poster presentation of the work at the Nuclear Fuels and Structural Materials (NFSM) symposium held in conjunction with American Nuclear Society Annual Conference in Anaheim in June 2008.

RESEARCH ACCOMPLISHMENTS

1. Alloy Sectioning and Metallographic Preparation:

Samples of the three alloys (Zirlo, NF 616, and 316 austenitic stainless steel) were sectioned into rectangular strips 1.25”x0.5” with either a diamond saw or electro-discharge machining (EDM). The size of the samples was critical in order to ensure that it fits into the holder of the supercritical water corrosion cell at the University of Wisconsin. These methods of cutting employed minimize the heating and/or excessive deformation of the samples, which could alter their microstructure and corrosion response. In addition, holes were drilled on either end of the strips in order to facilitate fixturing in the corrosion holder. Figures 1 (a) and (b) show samples of NF616 and 316 austenitic stainless steel, respectively, as examples of samples that were prepared for surface modification and testing work.

(a) **(b)**

Figure 1. Samples of alloys sectioned to appropriate size and drilled for surface treatment and testing work (a) NF616 ferritic-martensitic steel and (b) 316 austenitic stainless steel.

Following sectioning, the alloys were metallographically prepared by progressively grinding with silicon-carbide starting with 320, 400, 600, and 800 grit size silicon carbide papers. The samples for the cold spray surface treatment at Westinghouse were ground to a coarser surface finish (400 grit) because in the cold spraying process, coating adhesion to an extent depends on the surface roughness of the substrate. For the ion-based surface treatment at Sandia, the samples were ground to 800 grit size. Figure 2 show examples of the surface topography of the samples for the two types of surface treatment.

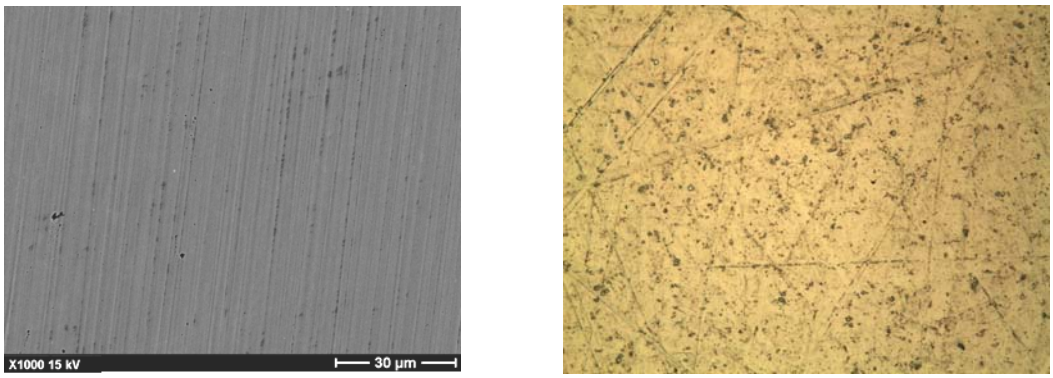

(a) **(b)**

Figure 2. Surface topography of samples (NF616 shown here as an example), (a) 800 grit surface finish for Sandia’s IBEST surface treatment and (ii) 400 grit surface finish for Westinghouse’s cold spray surface treatment process.

2. Cold-spraying of zirconium-diboride:

Cold-spray surface treatment, involving coating of zirconium-diboride 1 to 2 μm thick was performed at Westinghouse using their trade-marked SIMAT process. Westinghouse is an integral member of this NEER project. This work was done in two phases. The first phase involved cold-spraying zirconium-diboride on 3mm disks of Zirlo alloy at two different temperatures (temperatures were substantially lower than the traditional thermal spraying to be still categorized as cold spraying). The second phase involved cold-spraying of the three alloys, Zirlo, NF 616, and 316 austenitic stainless steel under optimized spraying conditions. All samples were coated on both sides. Figure 3 shows the spray gun facility at Westinghouse Corporation.

Figure 3. Cold spray facility at Westinghouse Corporation used for cold spraying zirconium-diboride coatings on various alloy substrates used in this study.

3. IBEST treatment for incorporation of boron and multilayered Zr/Gd structures at the surfaces of fuel cladding materials:

Ion **BE**am **S**urface **T**reatment (IBEST), an energetic ion-based surface treatment has been developed at Sandia National Laboratories, Albuquerque, NM based on the pioneering work performed in the former Soviet Union, Japan, and Cornell University. The process involves the impingement high energy (500 to 700kV) pulsed ion beam on a material surface with ion beams of gases such as H, He, N_2, O_2, Ne, Ar, Xe, Kr, CH_4. The energy imparted on the materials surface (1 to 6 J/cm^2) and current densities (250 A/cm^2) can be quite high and significant enough to cause melting in the near-surface regions of the material. Subsequent heat conduction into the substrate leads to rapid solidification of this melt zone at very high quench rates. The cooling rates, estimated based on melting and liquid diffusion models can be as high 10^9K/sec. This rapid cooling can lead to the material being "frozen-in" in novel states such as metastable alloys, nanocrystalline structures (e.g., grain refinement), supersaturated phases, and compositionally homogenized structures. The key technological strength of the IBEST treatment is the creation and localization of a pulsed high temperature and high pressure state. This technique can be used to incorporate or alloy elements such as boron or gadolinium which are largely insoluble in fuel cladding materials. Figures 4 shows the concept underlying the IBEST developed at Sandia National Laboratories.

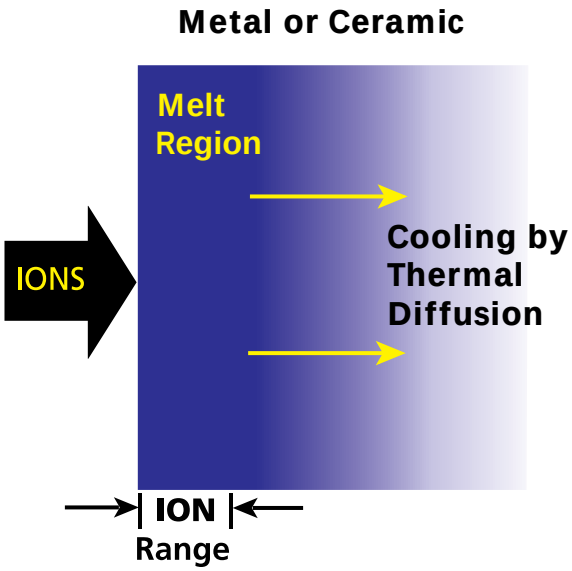

Figure 4. Concept underlying the IBEST process developed at Sandia National Laboratories, that was used for the for this NEER project.

Typical IBEST process parameters used for this research are summarized in Table 1.

Table 1. Summary of the important IBEST process parameters used in this research.

Parameter	**Value**
IFBA Sputter film thickness	500 to 750 nm
Accelerating voltage	700kV
Energy	3 to 4 J/cm^2 per pulse
Total number of pulses	25
Ion species	Nitrogen
Pulse width	150 ns
Shot Rate	1 per 15 seconds

3. Modeling of the IBEST process using 1-D mixing dynamics simulations:

To support our experimental work on surface alloying of boron into fuel cladding materials by the energetic ion process, IBEST, computational modeling was performed in order to predict process conditions that will yield the desired structural changes at the surface. The 1-D mixing dynamics simulations allowed us to predict the thickness of the surface melt layer, the duration for which the surface remains in the liquid state and the surface temperature during the IBEST process. These outcomes in turn allowed for the prediction of the thickness of the sputtered boron layer (or zirconium/gadolinium multilayers) that must be deposited in order to achieve the desired surface alloying by taking into account the effects of diffusion in the liquid layer, ablation, and surface evaporation. For example, if the sputter film thickness was excessive and/or the IBEST process conditions were not severe, inadequate alloying will result leading to a pure boron layer on the surface. On the other hand, if the sputtered film thickness is inadequate and the IBEST conditions are aggressive, ablation of the boron film will occur resulting in insufficient

boron incorporation into the substrate. Figure 5 shows the results of such simulations for a 0.5µm layer of boron on Zirlo and ferritic steel NF616. The following general conclusions can be drawn from these simulations:

- Boron surface temperature exceeds vaporization temperature for 400-600 ns at 6 J/cm^2

- Boron layer fully melts in both cases for at least 1.5 µsec

- Thinner NF616 melt layer (compared to Zirlo) due to higher thermal conductivity

- Up to 0.15 micron boron ablated per pulse at 6J/cm^2.

- RT (4Dt) diffusion scaling, with t ~ 3 µsec, D ~ 5e-4 cm$^{2/}$sec, yields ~ 1 µm diffusion length; therefore liquid phase diffusion outruns ablation.

Similar simulations were performed to decide the parameters for the subsequent IBEST experiments in the this research.

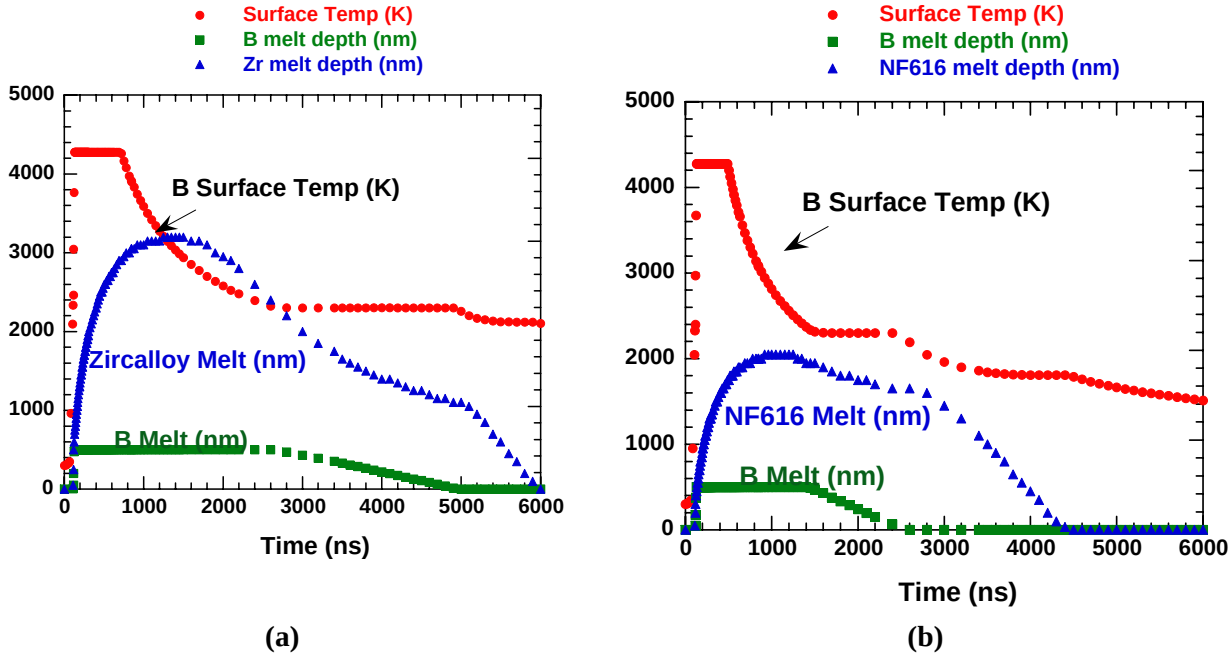

Figure 5. 1-D mixing dynamics simulations for 0.5µm boron film on (a) Zirlo and (b) NF616 ferritic steel. Nitrogen beam at 6 J/cm2 and beam pulse from from 0 - 300 ns were used for this simulation.

4. Characterization of As-Cold Sprayed Samples:

4.1 SEM Examination of 3mm disks of Zirlo cold sprayed with zirconium-diboride:

Scanning electron microscopy was performed to characterize the zirconium-diboride coatings that were cold sprayed on 3mm disk samples of Zirlo alloy. Cold spraying was performed at low and high temperatures, in order to evaluate the effects of temperature on the integrity of the coating. It should be noted here that low temperature refers to near-room temperature and high temperature refers to slightly higher temperatures (but substantially lower than temperatures used in thermal spraying). Figure 6 and 7 show scanning electron microscopy surface images of the zirconium-diboride coatings sprayed at the two temperatures. The coatings are uniform and dense and devoid of any delamination. Figure 8 and 9 show cross-sectional SEM images of the

zirconium-diboride coated Zirlo samples, for low and high temperature spraying, respectively, and the corresponding EDS (Energy Dispersive Spectroscopy) line scans for elements Zr and O. Boron is too light to be detected by the SEM-EDS technique. The SEM images in Figures 8 and 9 clearly show a zirconium-diboride layer 3 to 5μm thick. The EDS line scans support this in that a slight but sudden drop in Zr content is observed at the coating substrate interface. Figure 10 shows a 3mm disk of Zirlo sample coated with zirconium-diboride using Westinghouse's cold spray process. The important conclusions that can be derived from SEM analysis are: (a) a uniform dense coating of zirconium-diboride 3 to 5μm thick can be successfully deposited by using the cold spray process, (b) the coating adheres well to the substrate, and (c) for the two spray temperatures used there is no significant difference in morphology or thickness of the zirconium-diboride coating.

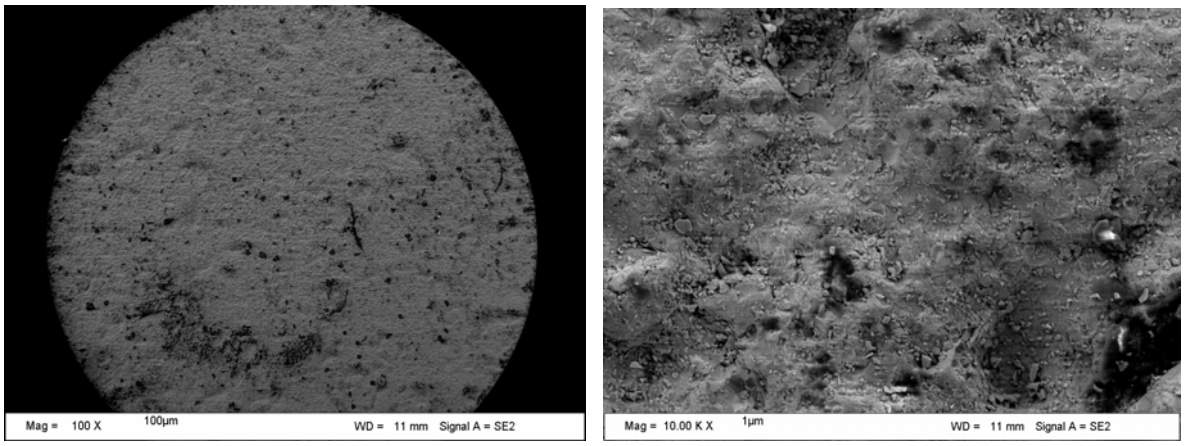

(a) 100X **(b) 10,000X**

Figure 6. Surface of the zirconium-diboride coating sprayed at low temperature on Zirlo samples.

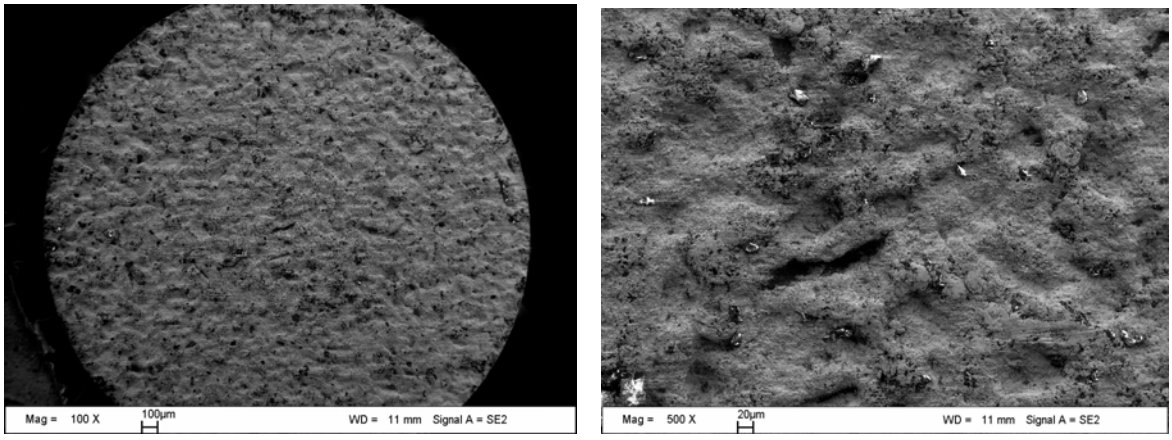

(a) 100X **(b) 10,000X**

Figure 7. Surface of the zirconium-diboride coating sprayed at a slightly higher temperature on Zirlo samples.

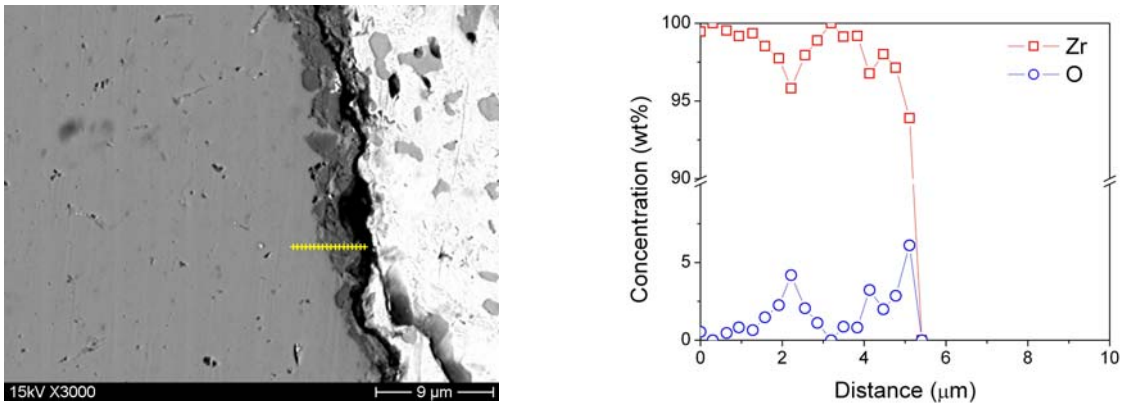

Figure 8. Cross-sectional SEM image (3000X) of the zirconium-diboride coating sprayed at low temperature on Zirlo samples and corresponding SEM-EDS line scan analysis.

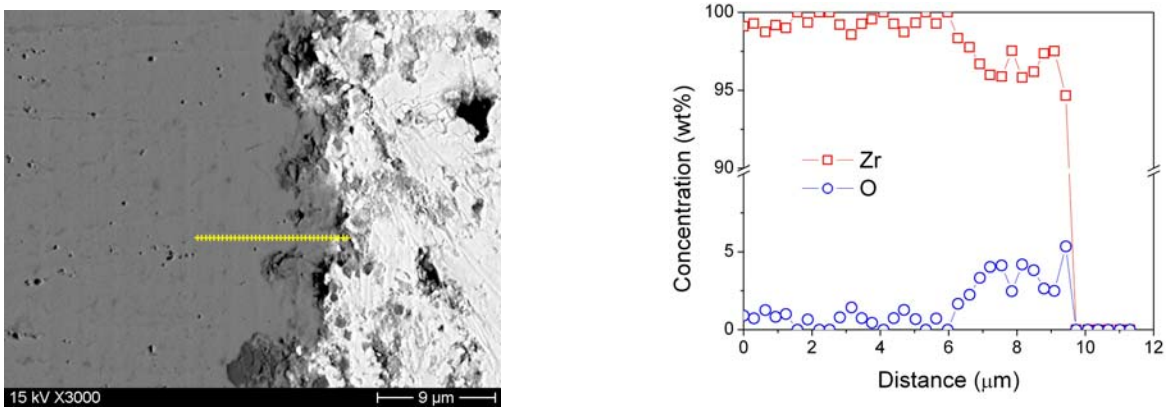

Figure 9. Cross-sectional SEM image (3000X) of the zirconium-diboride coating sprayed at a slightly higher temperature on Zirlo samples and corresponding SEM-EDS line scan analysis.

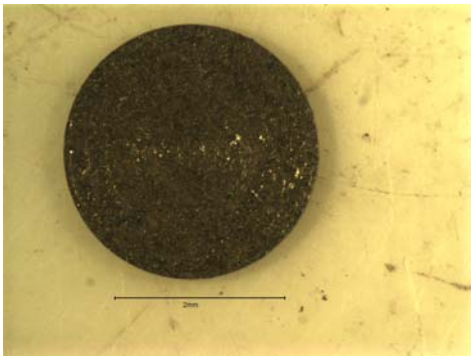

Figure 10. 3mm disk of Zirlo sample coated with zirconium-diboride using Westinghouse's cold spray process. A number of such samples, including control, and IBEST surface alloyed samples have been sent to Idaho National Laboratory for radiation testing.

4.2 Characterization of cold sprayed samples of Zirlo, NF616 and 316 stainless steel samples:

Figure 11 (a) to (f) shows the SEM surface images and EDS analysis of the surface of the cold sprayed samples of 316 stainless steel, NF616 ferritic steel, and Zirlo, respectively. The surfaces clearly show a coating with extensive deformation as would be expected of high velocity impact cold sprayed samples. The coatings are very similar in morphology for all three substrates. For 316 stainless steel and NF616 ferritic steel both show Fe and Cr from the underlying substrate indicating that the coatings are only about 1 to 2μm thick. Boron could not be detected by EDS because of its low atomic number and oxygen is observed because the cold sprayed process was conducted in air. All surfaces are made up of a uniform ZrB_2 coating.

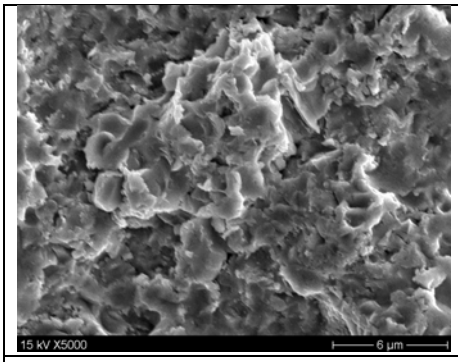

(a)

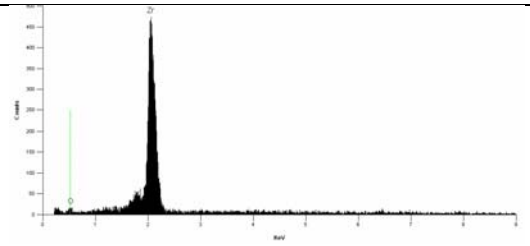

Cr: 6.25%, Fe: 25.08%, Zr: 61.47%, O: 7.21% (wt.%)

(b)

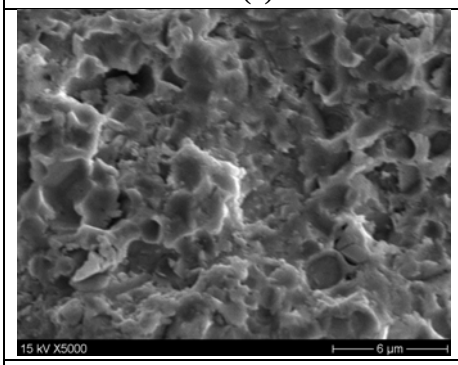

(c)

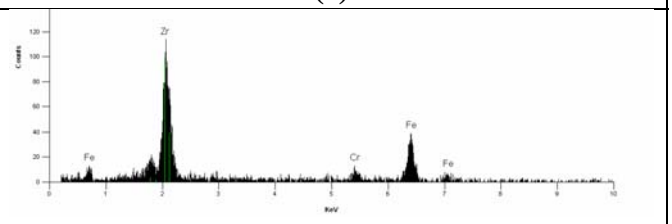

Cr: 4.38%, Fe: 33.83%, Zr: 54.40%, O: 7.39% (wt.%)

(d)

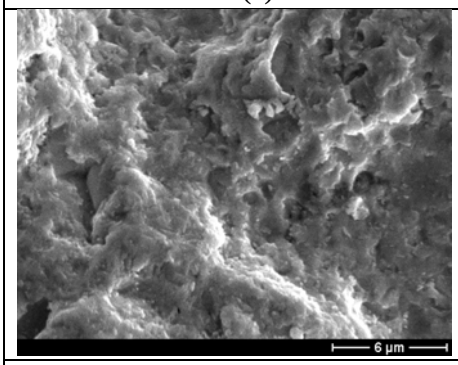

(e)

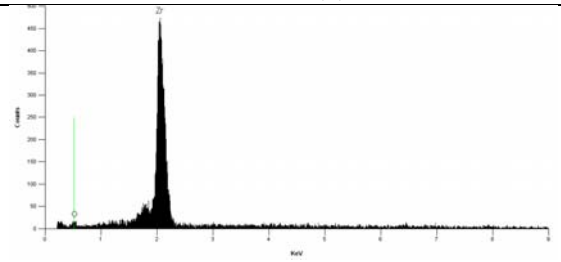

Zr: 91.51%, O: 8.49%

(f)

Figure 11. SEM surface images of ZrB_2 coated samples and corresponding EDS spectra, (a) & (b) 316 stainless steel, (c) & (d) NF616 ferritic steel, and (e) & (f) Zirlo.

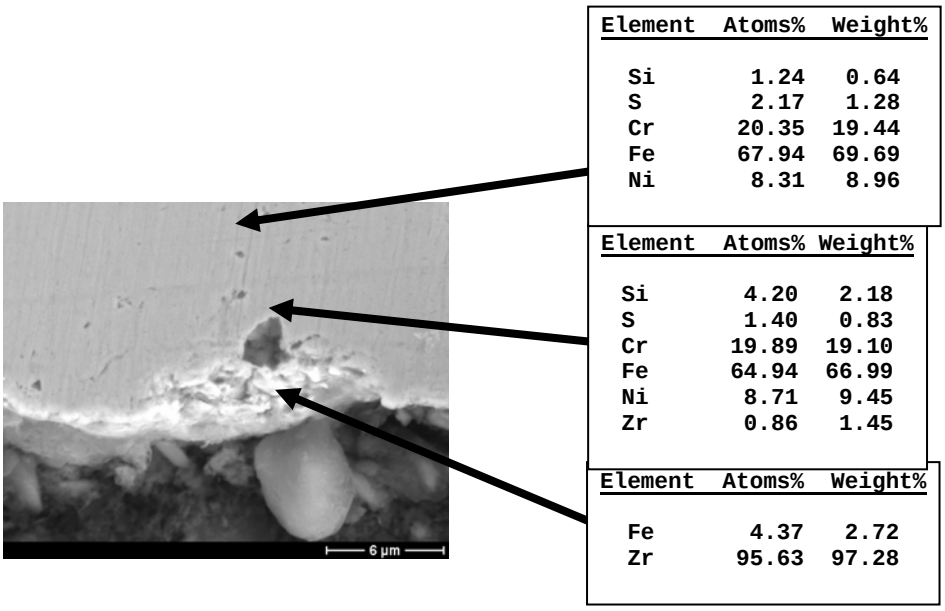

Figure 12. SEM cross-sectional image of cold sprayed ZrB_2 coating on 316 stainless steel and results of EDS compositional analysis at various locations.

Figure 12 shows the cross sectional SEM image of cold sprayed ZrB_2 coating on 316 stainless steel and results of EDS compositional analysis at various locations. The surface clearly shows a very thin well-adhered ZrB_2 coating about 1 to 2 µm thick. The substrate is heavily deformed as would be typical of the cold sprayed process. The surface analysis shows the presences of Zr from the cold sprayed coating but there is some evidence of Fe indicating the possibility of a metallurgical bond.

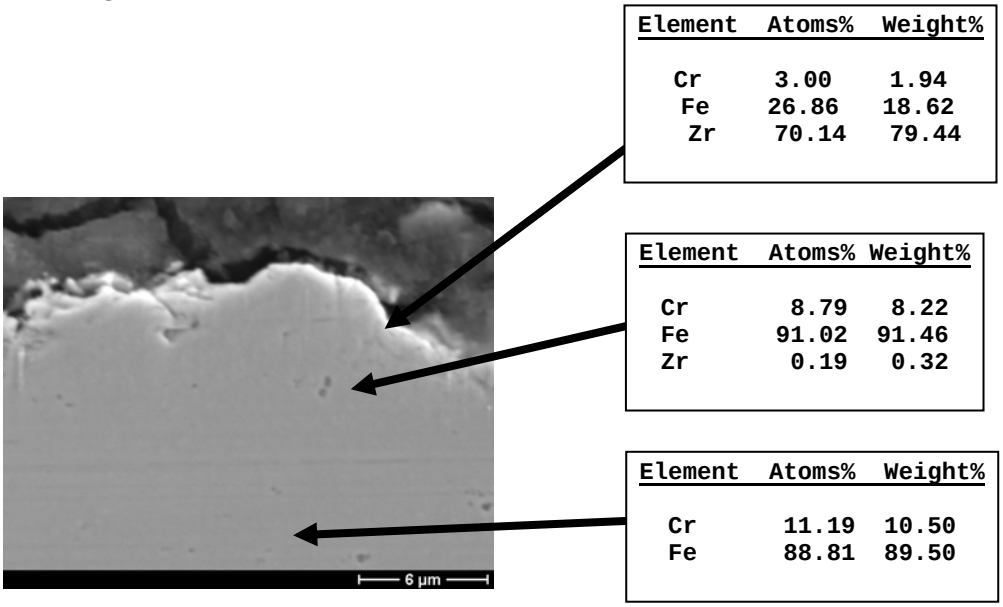

Figure 13. SEM cross-sectional image of cold sprayed ZrB_2 coating on NF616 and results of EDS compositional analysis at various locations.

Cross-sectional SEM image of cold sprayed ZrB_2 coating on NF616 ferritic steel (Figure 13) shows a heavily deformed structure, typical of cold sprayed structure, and there seems to be no sharp interface between the coating and the substrate, indicating that a metallurgical bond may have been created due to intense plastic deformation and localized heating. This bodes well for the mechanical stability of the coating particularly at high temperatures.

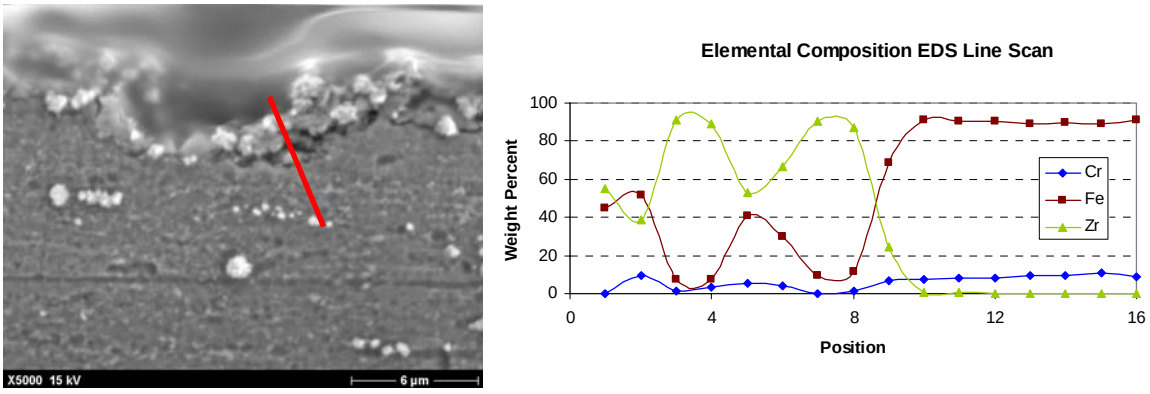

Figure 14. SEM cross-sectional image of cold sprayed ZrB_2 coating on NF616 and EDS compositional line scan which is indicative of a metallurgical bond.

Figure 14 shows the SEM cross sectional image of cold sprayed ZrB_2 coating on NF616 and results of an EDS compositional line scan. The EDS shows fluctuating Fe and Zr concentrations caused by roughness of the substrate. The sinusoidal variations in these compositions are indicative of a good coating-substrate bond.

Figure 15 shows the cross-sectional SEM image of cold sprayed ZrB_2 coating on Zirlo. Again a cold worked structure is observed and the ZrB_2 coating seems to have formed an excellent metallurgical bond with the Zirlo substrate.

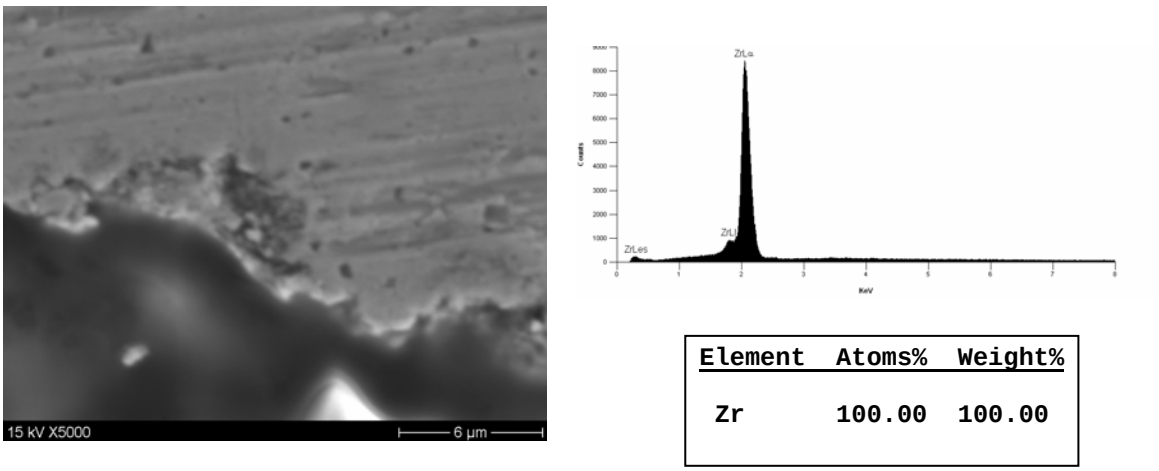

Element	Atoms%	Weight%
Zr	100.00	100.00

Figure 15. SEM cross sectional image of cold sprayed ZrB_2 coating on Zirlo and EDS spectra taken at the surface.

Grazing incidence x-ray diffraction analysis of the cold sprayed samples for all three substrates confirmed the presence of a ZrB_2 coating. The results of x-ray diffraction analysis for all three substrates are shown in Figure 16.

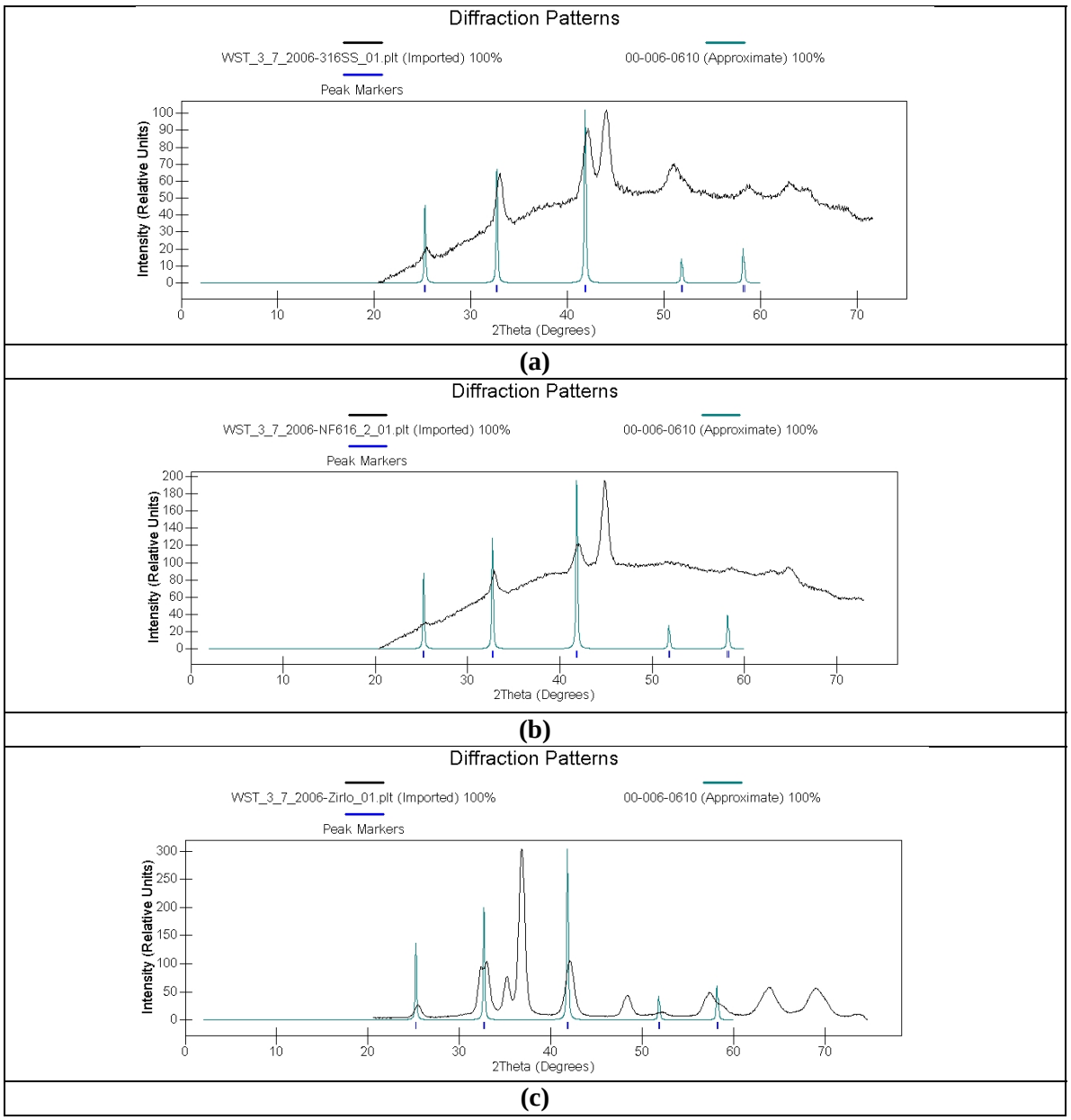

Figure 16. Grazing incidence x-ray diffraction of ZrB_2 cold spray coated substrates showing the presence of ZrB_2 phase. Peaks shown in blue are the standard peaks for ZrB_2. (a) 316 stainless ateel, 9b) NF616 ferritic steel, and (c) Zirlo.

5. Characterization of IBEST surface treated samples:

The as-received IBEST samples were characterized in detail using scanning electron microscopy (both plan and cross-sectional imaging) and x-ray diffraction. In all cases it was noted that the boron film had completely alloyed into the substrate materials as a result of surface melting and subsequent rapid solidification induced by the IBEST process. This is noteworthy given that boron is thermodynamically immiscible in all three substrate materials at room temperature. Figure 17 shows the SEM plan view image of the 316 stainless steel samples after IBEST surface treatment and the EDS compositional spectrum taken on the surface. The Figure also shows EDS compositional analyses at three different locations on the surface. The SEM image shows a homogeneous microstructure with no evidence of compositional segregation having occurred during the IBEST treatment. The undulating surface structure is indicative of melting and subsequent solidification at very high cooling rates. Similar results were observed for NF616 ferritic steel (Figure 18) and Zirlo alloy (Figure 19). A 'rippled' or a 'puddled' surface morphology was observed on all samples which is indicative of the high rate of cooling of the melted surface layer.

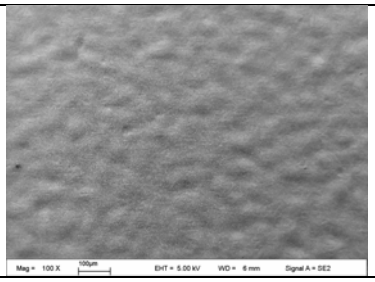

(a)

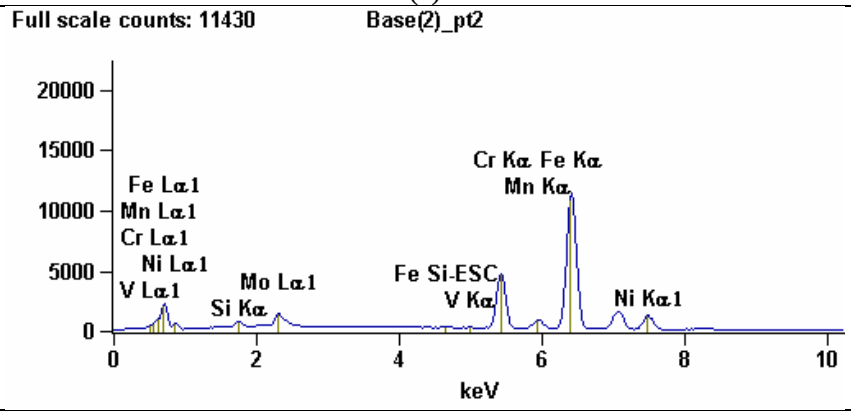

(b)

	Al	Si	V	Cr	Mn	Fe	Ni	Mo
pt1		1.75		18.17	0.96	66.30	10.21	2.60
pt2		2.05	0.19	17.88	0.91	66.21	9.86	2.89
pt3	0.15	1.67		18.41	1.03	66.94	9.82	1.97

(c)

Figure 17. Surface analyses of boron IBEST treated 316 austenitic stainless steel sample showing (a) SEM surface image, (b) a typical SEM EDS analysis of the surface, and (c) compositions measured at three different locations on the surface.

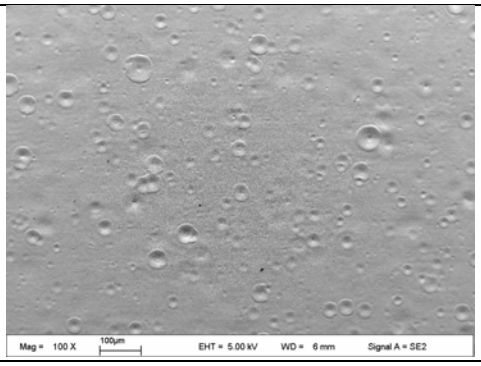

(a)

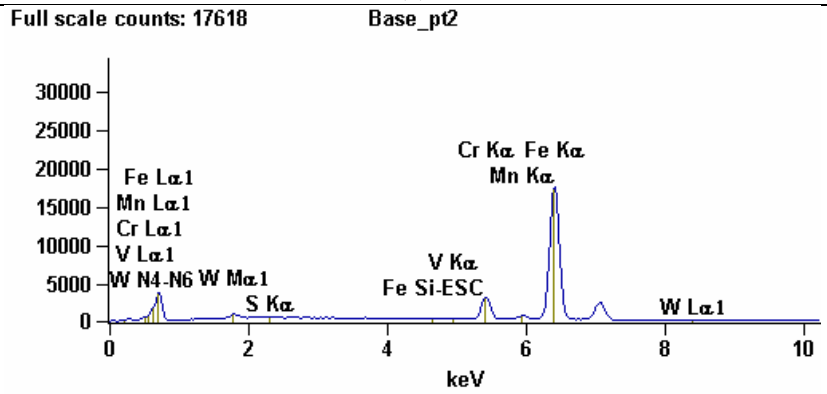

(b)

	S	V	Cr	Mn	Fe	Mo	W
pt1		0.27	10.22	0.62	87.36	0.43	1.09
pt2	0.47	0.24	9.44	0.49	88.57		0.78
pt3		0.23	10.12	0.54	88.21		0.90
pt4		0.24	9.56	0.53	88.53	0.32	0.82

(c)

Figure 18. Surface analyses of boron IBEST treated NF616 ferritic steel sample showing (a) SEM surface image, (b) a typical SEM EDS analysis of the surface, and (c) compositions measured at three different locations on the surface.

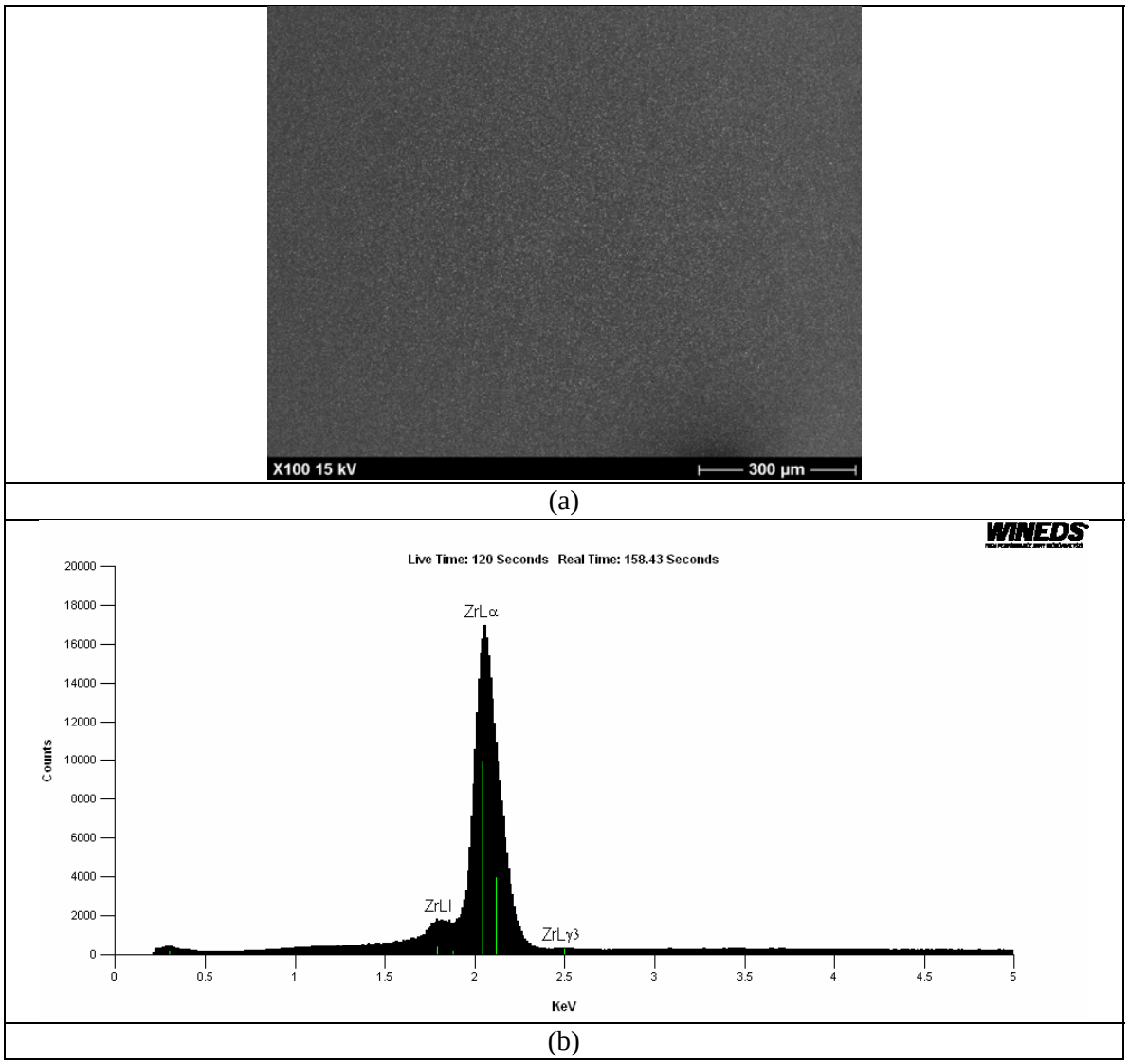

Figure 19. Surface analyses of boron IBEST treated Zirlo sample showing (a) SEM surface image, and (b) a typical SEM EDS analysis of the surface

SEM cross-sectional imaging of the IBEST treated samples is being performed. Figure 20 shows the cross-sectional SEM image of boron IBEST treated NF616 steel sample. A clear boron surface layer 3 to 4µm was clearly observed after etching the steel with Marble's reagent (H_2O 50 mL + HCl 50 mL + copper sulfate 10 grams). This layer represents the boron alloyed zone resulting from both surface melting and solid state diffusion during the IBEST treatment.

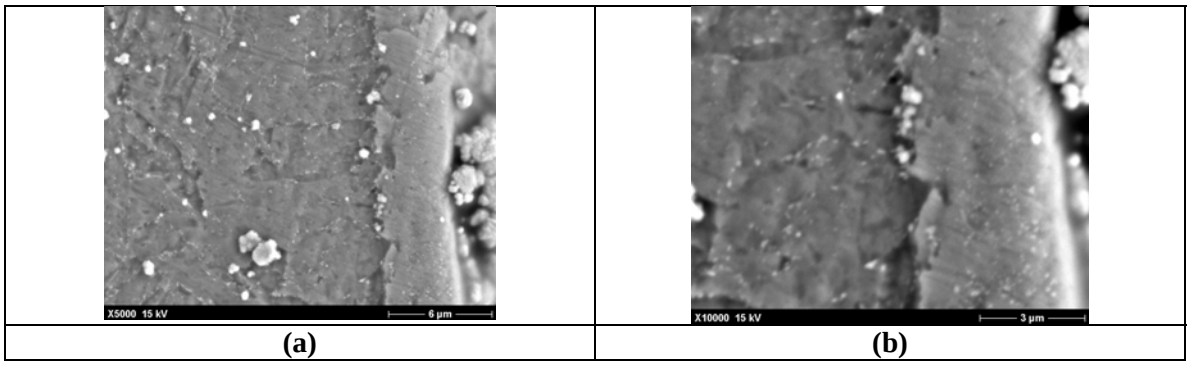

Figure 20. Cross-sectional SEM image of the boron-IBEST treated NF616 ferritic steel showing the boron-alloyed surface layer (Marble's reagent etchant: H_2O 50 mL + HCl 50 mL + copper sulfate 10 grams).

Figure 21 shows the results of the x-ray diffraction studies of the untreated and boron IBEST treated 316 stainless steel samples. The patterns are indicative of an austenitic phase and there is no evidence of second phase evolution (particularly borides) during the IBEST treatment. A slight shift in the various FCC peaks is observed after boron IBEST surface treatment and this may be indicative of lattice supersaturation resulting from forced incorporation of boron into the stainless steel.

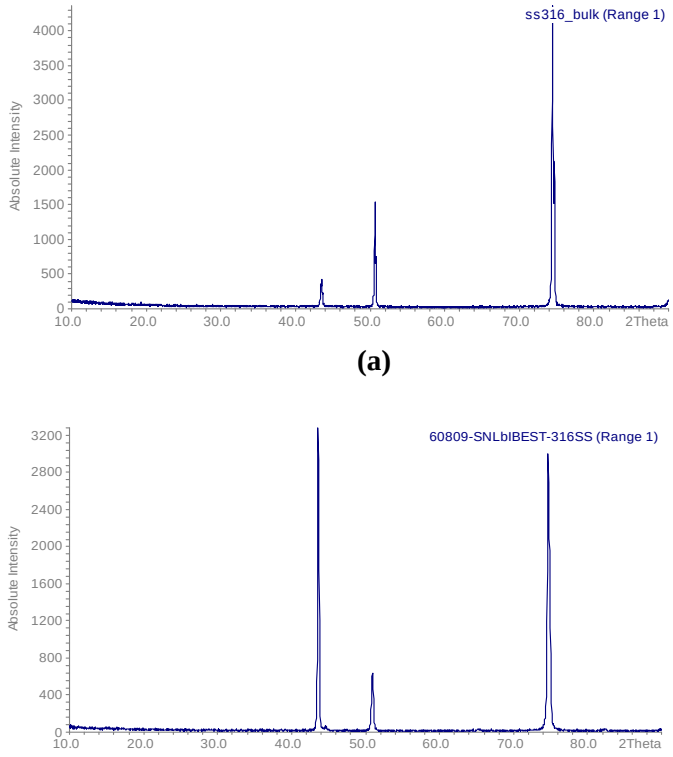

Figure 21. X-ray diffraction analysis of 316 austenitic stainless steel sample (top) and boron IBEST treated 316 austenitic stainless steel sample.

6. Supercritical water (SCW) corrosion testing:

Supercritical water corrosion tests were performed in the test facility at the University of Wisconsin. Testing was performed in supercritical water (SCW) at 500°C and containing 10 to 25 ppb dissolved oxygen for an exposure duration 165 hours. Figure 22 shows the SCW corrosion test equipment at the University of Wisconsin. Figure 23 shows the geometry of the corrosion test samples and the Inconel 625 corrosion sample holder (samples are fixtured with alumina washers to avoid galvanic corrosion between the sample and the holder). Figure 24 shows the temperature, pressure, and dissolved oxygen profiles that were monitored on-line during the high temperature SCW exposure.

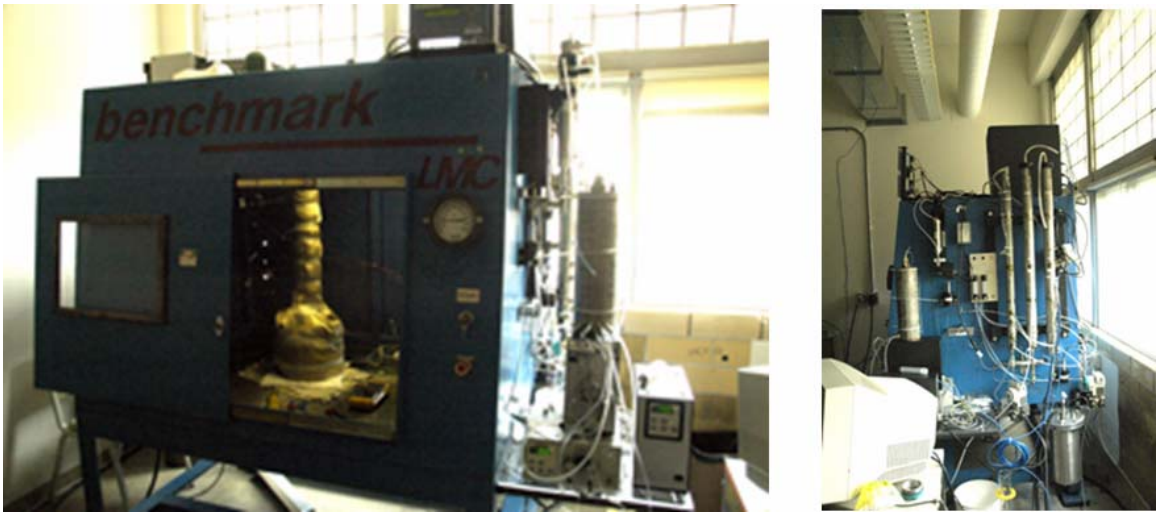

Figure 22. Supercritical water corrosion test facility at University of Wisconsin where the cold sprayed zirconium-diboride coatings were tested.

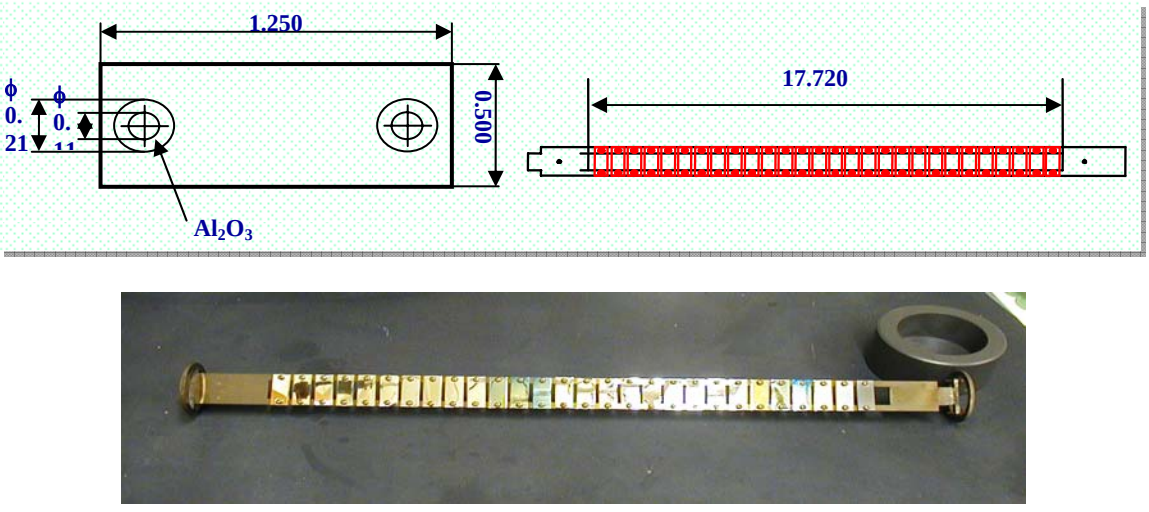

Figure 23. Sample geometry and design and the Inconel 625 corrosion sample holder, which can accommodate up to twenty eight samples.

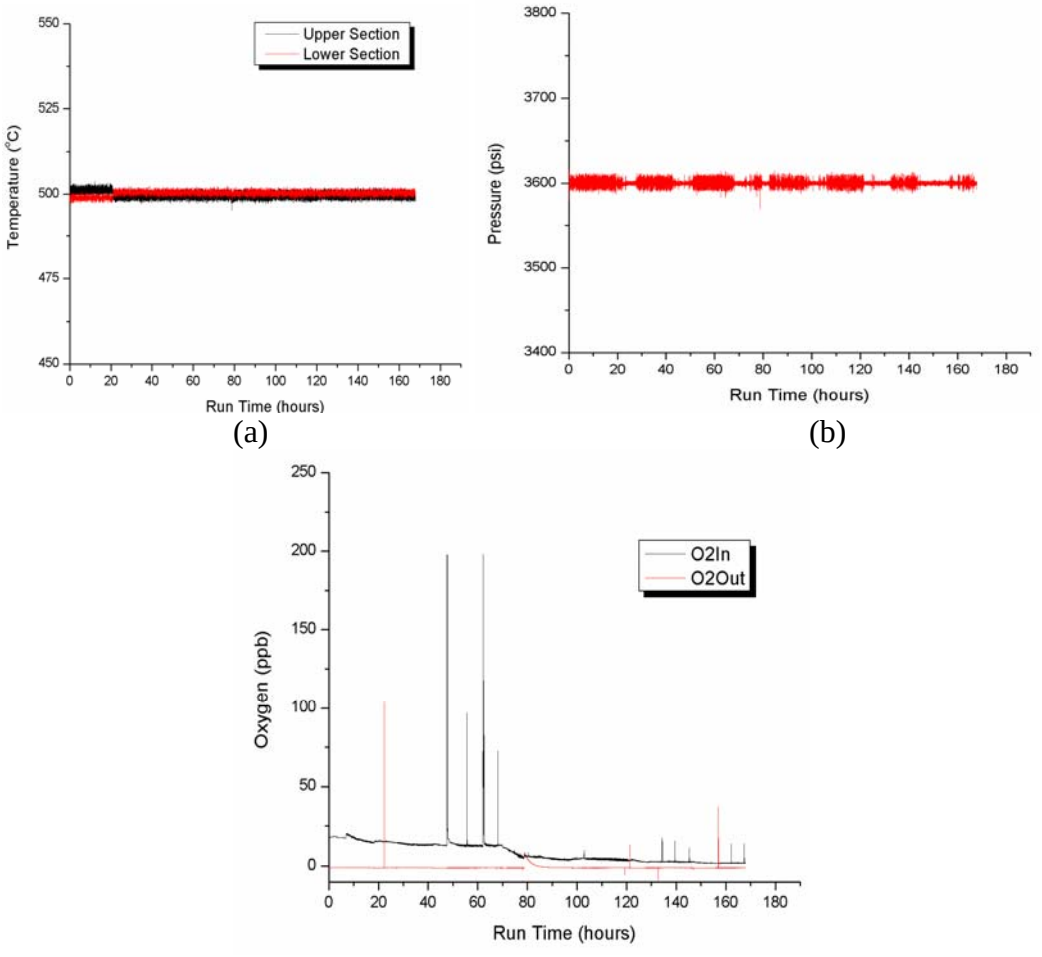

Figure 24. Temperature, pressure, and dissolved oxygen profiles that were monitored on-line during the SCW exposure at 500°C.

7. Characterization of cold sprayed samples after supercritical water testing:

After the supercritical water test, the samples were weighed (to examine weight gain as a measure of corrosion or oxidation) and SEM and x-ray diffraction analysis.

Figure 25 shows the SEM surface images of the as-sprayed 316 stainless steel sample and after exposure to supercritical water. Fine grains of oxide with a polyhedral morphology are observed on the surface. Figure 26 shows the EDS analysis of the surface of as-received 316 stainless steel and after exposure of the ZrB_2 coated 316 stainless steel samples after exposure to SCW. As maybe seen from Figure 26 (b), the ZrB_2 is largely intact after the corrosion test with major portion of the signals coming from the coating; however, some Fe and Cr oxides are also observed. There does not seem to be any delamination of the coating due to oxidation or due to thermal stresses. Similar observations can be made for NF616 ferritic steel, the results of which are shown in Figures 27 and 28.

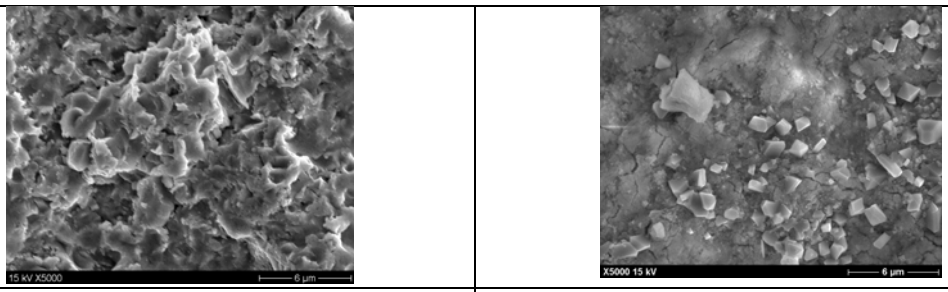

(a) **(b)**

Figure 25. SEM surface images of ZrB_2 cold sprayed samples on 316 stainless steel (a) as-sprayed and (b) after exposure to SCW water at 500^{o}C at 168 hours.

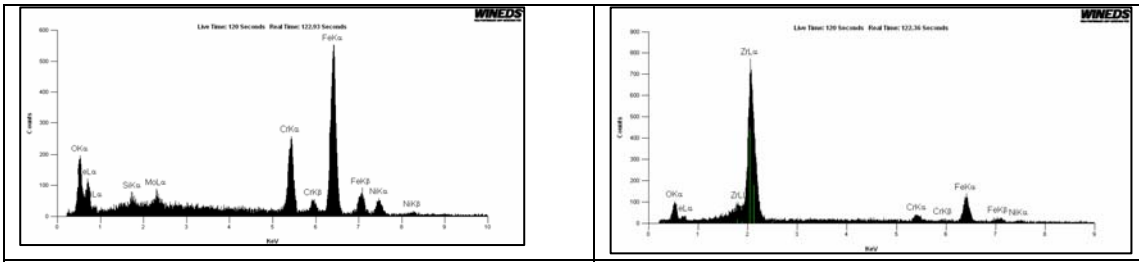

(a) **(b)**

Figure 26. SEM EDS analysis of (a) as-received 316 stainless steel and (b) ZrB2 coated 316 austenitic stainless steel sample after exposure to SCW test.

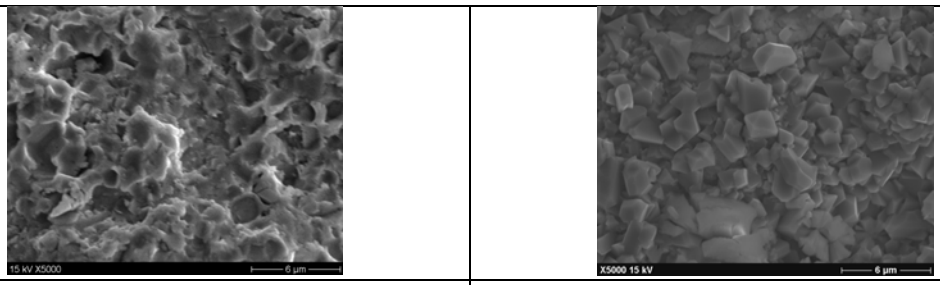

(a) **(b)**

Figure 27. SEM surface images of ZrB_2 cold sprayed samples on NF 616 ferritic steel (a) as-sprayed and (b) after exposure to SCW water at 500^{o}C at 168 hours.

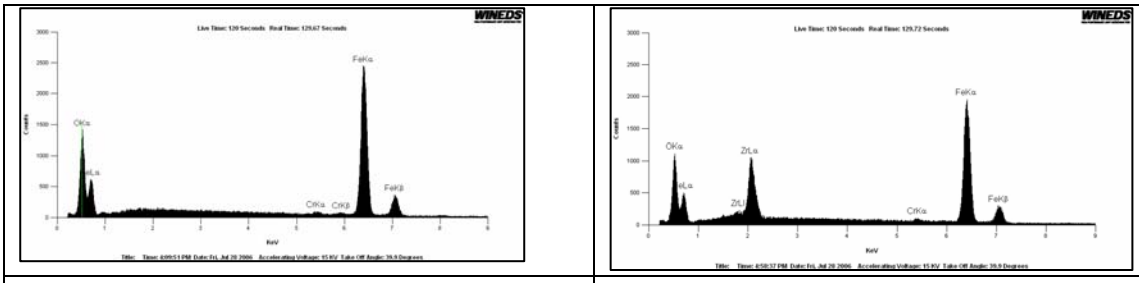

Figure 28. SEM EDS analysis of (a) as-received NF616 ferritic steel and (b) ZrB2 coated 316 austenitic stainless steel sample after exposure to SCW test.

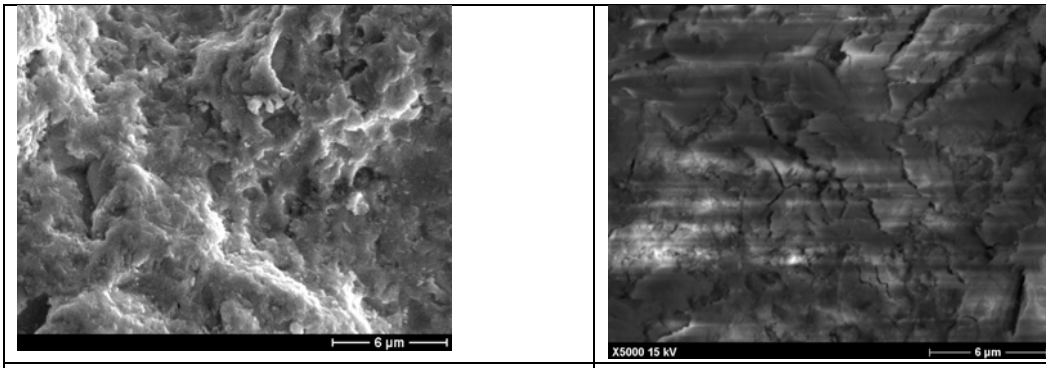

(a) **(b)**

Figure 29. SEM surface images of ZrB_2 cold sprayed samples on Zirlo (a) as-sprayed and (b) after exposure to SCW water at 500°C at 168 hours.

For the ZrB_2 cold spray coated Zirlo samples, the oxide morphology is considerably different compared those observed for 316 stainless steel and NF 616 ferritic steel samples (Figure 29). The oxide layer seems to have a more uniform morphology compared to the discrete polyhedral morphology observed observed for the two steels. This appears to indicate that the underlying substrate dictates the oxide morphology, which is not unexpected given the shallow thickness and porosity in the coatings.

SEM cross sectional image and cross-sectional EDS line scan of the ZrB_2 cold sprayed NF616 samples after exposure to SCW, does not show any significant oxidation, and it can be seen semi-quanitatively that ZrB_2 coating is still present.

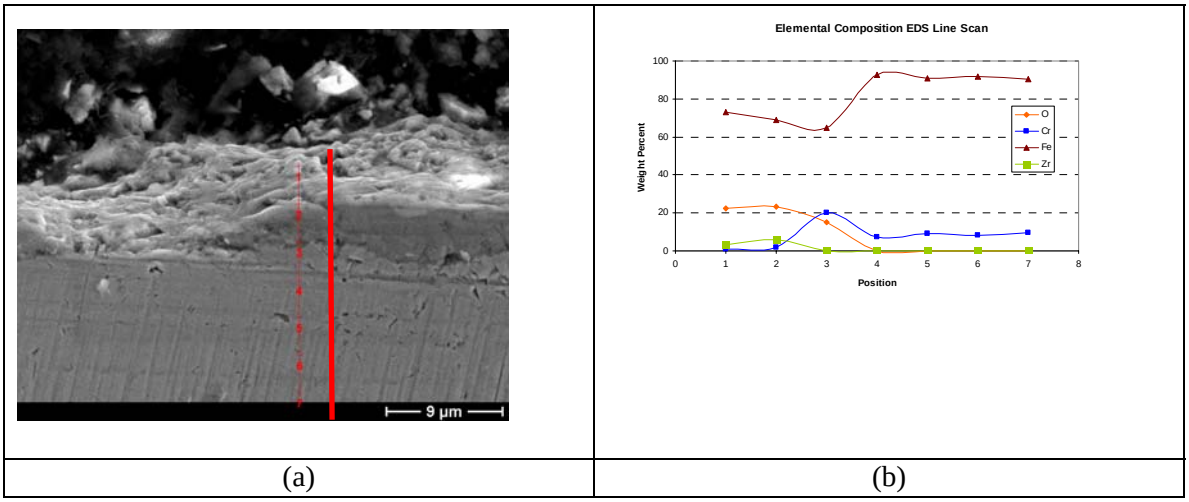

(a) (b)

Figure 30. (a) SEM cross sectional image of the ZrB2 coated NF616 ferritic steel samples after exposure to supercritical water test (b) EDS line scan across the surface layer.

Figure 31 shows x-ray diffraction patterns for ZrB_2 sprayed 316 austenitic stainless steel before and after exposure to supercritical water tests. After exposure to SCW, oxide peaks emerge and these oxides have been identified to be oxides of Fe, Cr, and Zr. No boron oxide peaks were observed, indicating that ZrB_2 remains chemically stable in 500°C SCW.

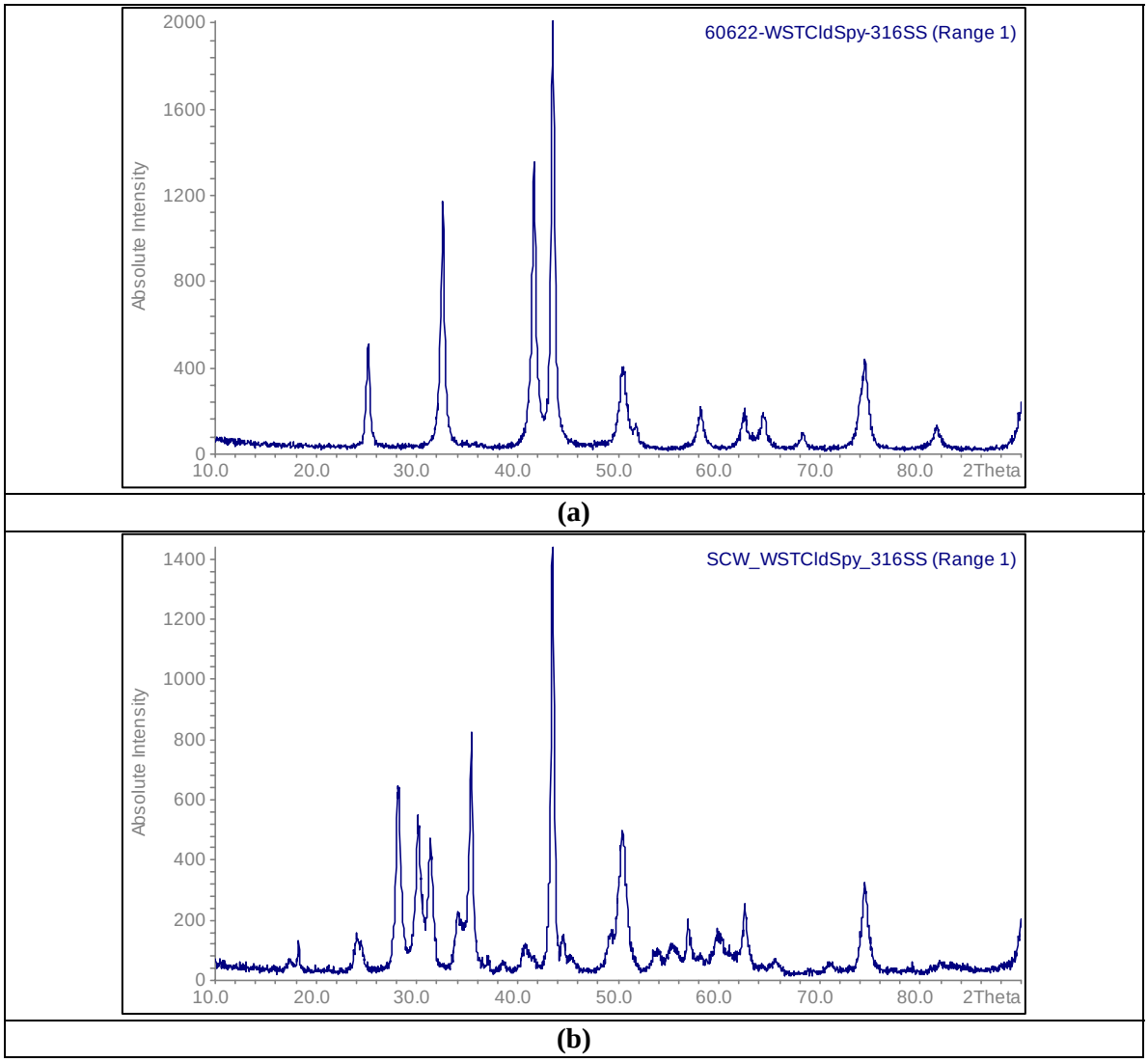

Figure 31. X-ray diffcation patterns of (a) ZrB_2 sprayed 316 austenitic stainless steel and (b) sample in (a) exposed to SCW at 500°C for 165 hours.

8. Characterization of IBEST treated samples after supercritical water testing:

Figure 32 shows SEM surface images of control boron-IBEST treated samples and after exposure of these samples in SCW at 500°C for 165 hours. For both NF616 ferritic steel and 316 stainless steel the morphology of the oxide particles does not change after IBEST treatment, but there is a higher density of oxide particles for the IBEST treated samples. The surface oxide morphology for IBEST treated Zirlo is substantially different from both NF616 ferritic steel and 316 stainless steel, in that a more uniform surface oxide forms on the surface. The oxide morphology for IBEST treated samples closely replicates that of the substrate material.

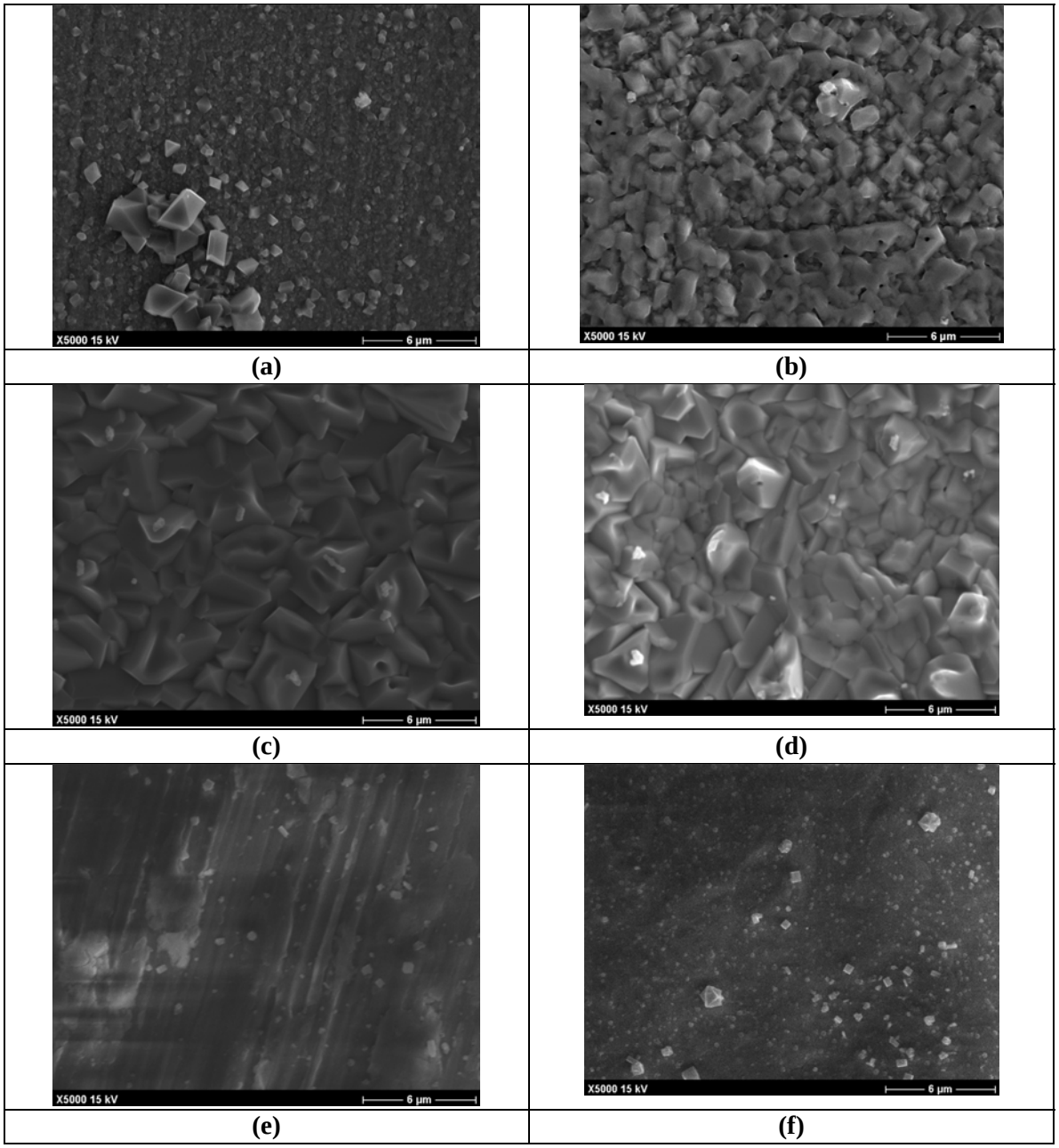

Figure 32. (a), (c), and (e) surface SEM images of 316 austenitic stainless steel, NF616 ferritic steel, and Zirlo after exposure to SCW at 500°C for 165 hours and (b), (d), and (f) surface SEM images of boron-IBEST treated 316 austenitic stainless steel, NF616 ferritic steel, and Zirlo after exposure to SCW at 500°C for 165 hours.

Figure 33 shows cross-sectional SEM image of boron IBEST treated NF616 ferritic steel after exposure to SCW at 500°C for 165 hours. An oxide layer clearly develops on the surface, but it is similar in thickness to the oxide layer that would develop on NF616 without the surface treatment. EDS line scan shows an outer magnetite layer and an inner (Fe, Cr) spinel oxide layer. This trend is very similar to those observed in non-surface treated NF616 ferritic steel. Boron could not be detected by EDS because of its low atomic number.

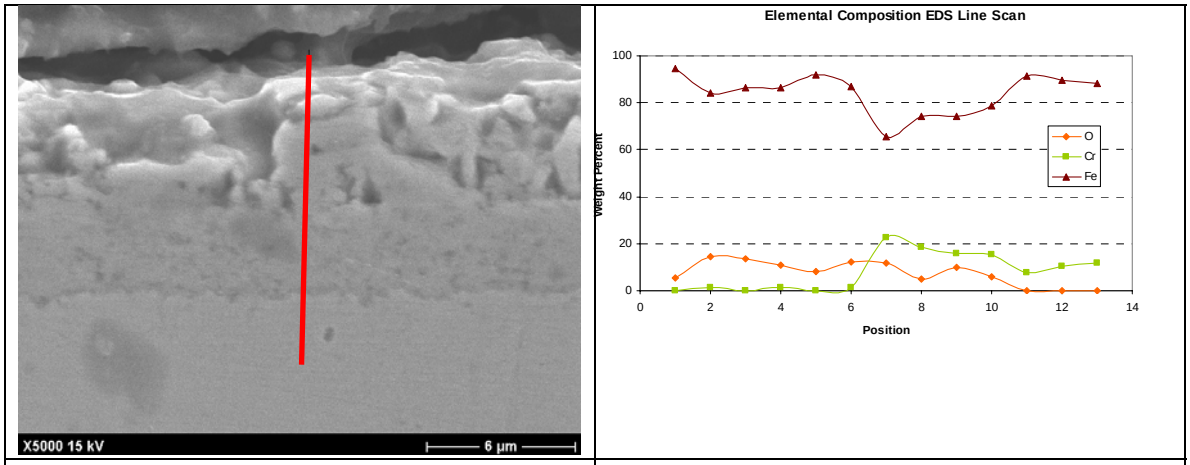

(a) (b)

Figure 33. (a) cross-sectional SEM image of the boron IBEST treated NF616 ferritic steel after exposure to supercritical water at 500°C for 168 hours and (b) EDS line scan across the oxide layer.

X-ray diffraction patterns for 316 austenitic stainless steel, B-IBEST treated 316 austenitic stainless steel, and B-IBEST treated 316 austenitic stainless steel – SCW exposed samples are shown in Figure 34. Boron IBEST treatment leads to leads to a slight increase in lattice parameter due to boron supersaturation. X-ray diffraction of the SCW samples clearly shows peaks of Fe and Cr-oxide and there was no evidence of any boron oxides on the surface.

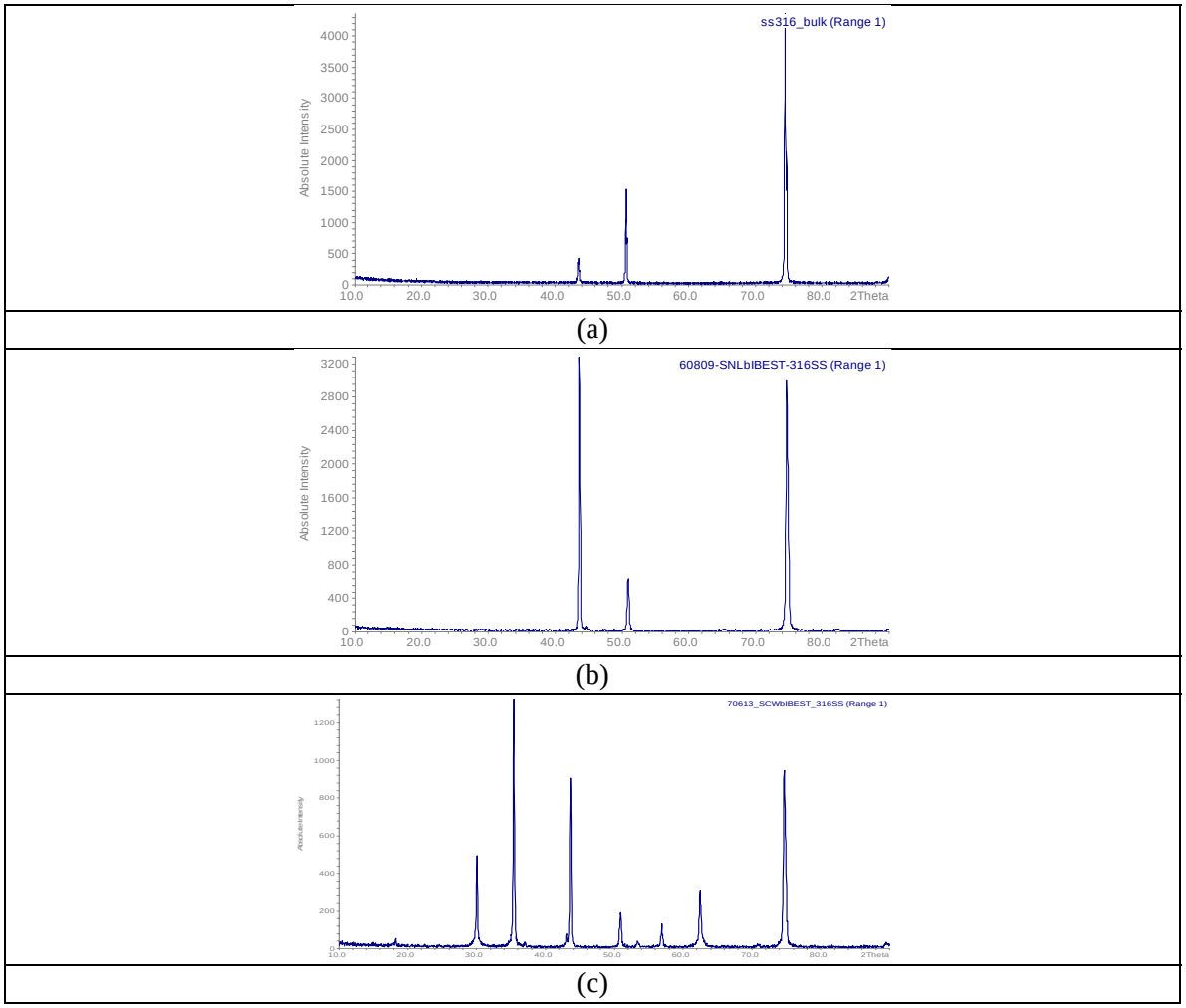

Figure 34. X-ray diffraction patterns for (a) 316 austenitic stainless steel, (b) B-IBEST treated 316 austenitic stainless steel, and (c) SCW exposed B-IBEST treated 316 austenitic stainless steel.

9. Autoclave testing of samples in steam environment

Autoclave testing of control samples of the three alloys, IBEST surface treated samples, and ZrB2 sprayed samples were tested in a steam autoclaves at Westinghouse Science and Technology, Pittsburgh, PA. Tests were performed at 427^{o}C at 100 atmospheres pressure for 165 hours. Figure 34 shows the autoclave testing facilities at Westinghouse where the samples were tested. The samples were cleaned as per Westinghouse procedures, weighed and suspended in sample racks and introduced into the autoclave.

7.6 liter stainless steel autoclave

Automated autoclave environment monitoring

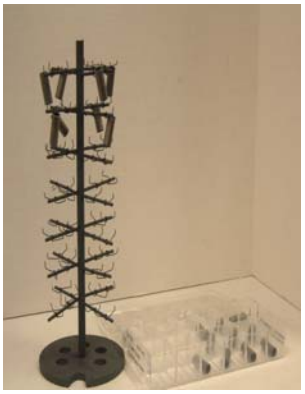

Specimen racks for suspending samples

Figure 34. Autoclave test facilities at Westinghouse where the samples were tested at 427°C at 100 atmospheres for 165 hours.

10. Characterization of cold sprayed samples after steam autoclave testing:

The cold spray coatings were comparable in their oxidation resistance to the uncoated substrates when tested in the steam autoclave environment. An example of this is shown in Figure 35, for NF 616 ferritic steel, which shows the cross-sectional SEM image of the ZrB2 coated NF616 ferritic steel sample, after steam autoclave testing. The corresponding EDS line-scan analysis is also shown. There is no significant growth of the surface due to oxidation and surface layer is adherent to the substrate. The EDS line-scan shows that there is clear diffusion of Fe through the ZrB_2 coating to form a thin outer magnetite layer. The ZrB_2 layer in the subsurface region underneath the magnetite layer.

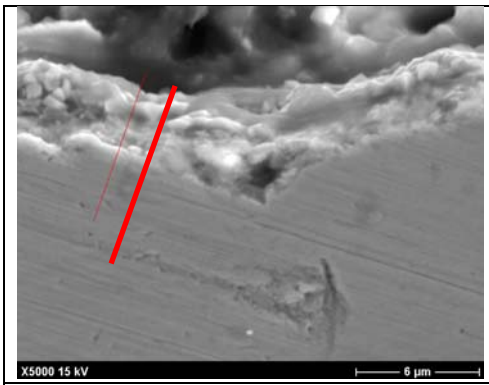

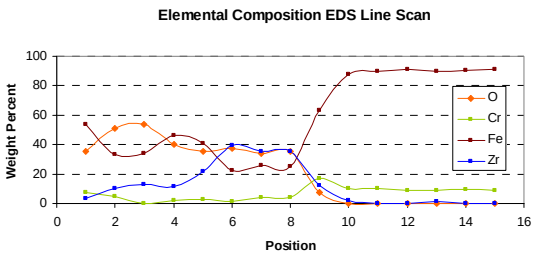

(a) **(b)**

Figure 35. (a) SEM cross-sectional image of the ZrB_2 spray coated NF616 ferritic steel after exposure to the steam autoclave test at 427°C (b) EDS line-scan analysis of the surface layer showing that the ZrB_2 coating is intact after the autoclave tests and the out-diffusion of Fe through the coating.

10. Characterization of IBEST treated samples after steam autoclave testing:

The IBEST surface treated samples showed corrosion performance similar to the uncoated substrate, in steam autoclave tests. EDS line scan analysis shows an outer magnetite layer and an inner (Fe, Cr) spinel oxide layer. Boron although present is not detectable by EDS analysis. It is important to point out here that this is a significant result, in that it shows that incorporation of boron into the surface of the steel by IBEST process does not adversely affect the corrosion resistance of this alloy. Similar observations were made for 316 stainless steel and Zirlo samples.

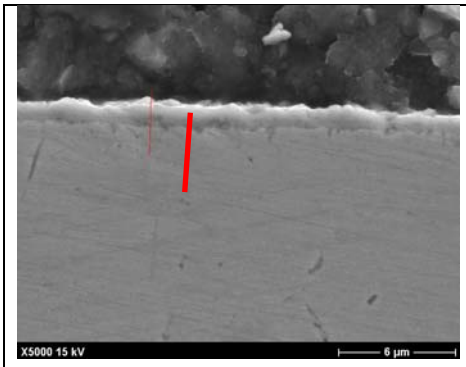

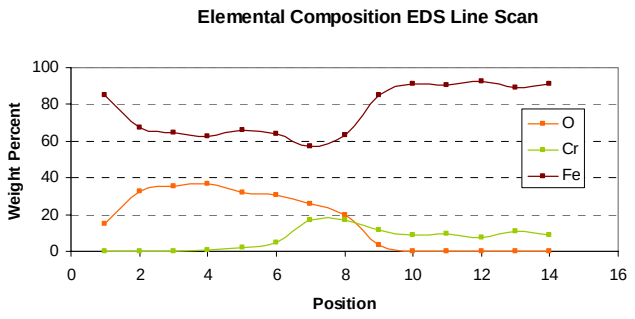

(a) **(b)**

Figure 36. (a) SEM cross-sectional image of the boron IBEST surface treated NF 616 ferritic steel after exposure to the steam autoclave test at 427°C (b) EDS line-scan analysis of the surface layer showing that the ZrB_2 coating is intact after the autoclave tests and the out-diffusion of Fe through the coating.

11. Evaluation of weight change after supercritical water tests at 500°C

Control, IBEST-treated and cold sprayed samples of Zirlo, NF616 ferritic steel and 316 austenitic stainless steel were tested in the University of Wisconsin supercritical water corrosion facility. These tests were performed at 500°C for 165 hours in SCW with 10 to 25 ppb dissolved oxygen. Figure 37 shows the weight gain measurements (per unit area of the sample) of all the samples tested. For 316 austenitic steel, which exhibits remarkably good corrosion resistance in SCW, the IBEST and cold spray surface treatments reduce the corrosion resistance to a small degree. For NF616 ferritic steel the surface treatments improve the corrosion resistance slightly, whereas for Zirlo, the surface treatments lead to a slight detriment in corrosion resistance. In general, surface treatments do not adversely affect the corrosion resistance of the three substrate materials. This is a significant result since the purpose of boron incorporated into the cladding material is to serve the role of a neutron absorber and the observation that such a surface treatment does not dramatically reduce the existing corrosion resistance of these materials is significant.

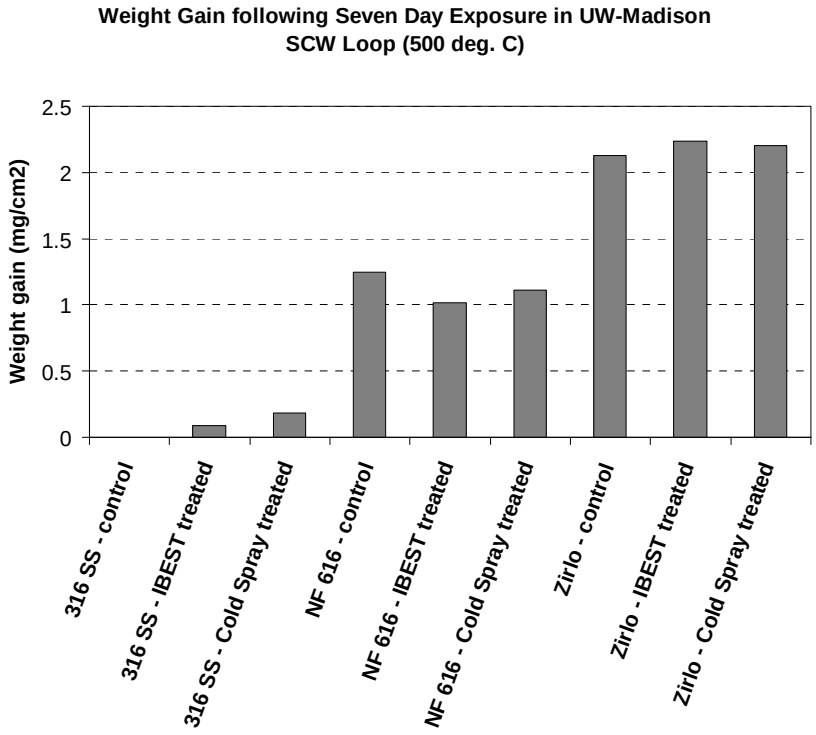

Figure 37. Weight gain (per unit area of ample) of Zirlo, NF616 ferritic steel, and 316 austenitic steel after exposure to supercritical water at 500^{o}C for 168 hours.

12. Evaluation of weight change after steam autoclave tests at 427^{o}C

Control, boron IBEST surface treated and zirconium diboride cold sprayed samples of 316 austenitic stainless steel, NF616 ferritic steel and Zirlo were subjected to steam autoclave tests at 427^{o}C for 168 hours, at Westinghouse Science and Technology Center, Pittsburgh. Results of weight gain measurements (per unit area of the sample surface) are summarized in Figure 38. For 316 stainless steel which exhibits remarkable corrosion resistance in SCW, the surface treatments marginally reduced the corrosion resistance. Fir NF616 steel the cold spray treatment improved the corrosion resistance, whereas for Zirlo alloy IBEST both surface treatments were detrimental to corrosion resistance with IBEST treatment performing slightly worse than cold sprayed samples. In general, the cold sprayed samples exhibited better corrosion resistance compared to the IBEST treatment.

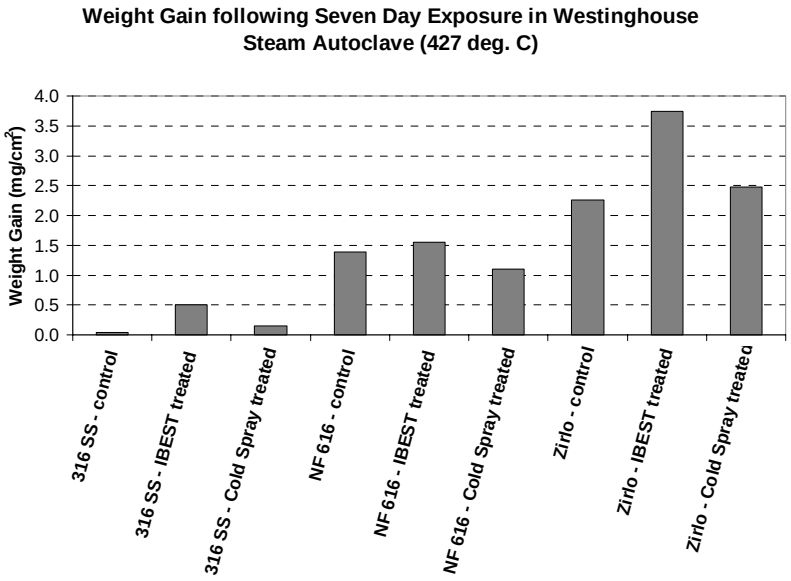

Figure 38. Results of weight gain measurements for control, boron IBEST surface treated, and zirconium diboride cold sprayed samples of 316 austenitic stainless steel, NF616 ferritic steel and Zirlo samples after steam autoclave tests (performed at Westinghouse) at 427^{o}C for 165 hours.

13. Multi-layered surface treatment:

Our prior experiments on incorporating gadolinium, another commonly used IFBA element into Zirlo using Sandia's IBEST process were successful, in so far as alloying Gd into Zr against thermodynamic restrictions. Up to about 30 at.%Gd was alloyed into Zr up to depths of about 2 to 3 μm using ion energies of about 2J/cm^2. However, upon exposure to steam autoclave environment at 800°F, for just 24 hours, the Gd-alloyed Zirlo exhibited 2 to 3 times weight gain due to oxidation compared to the control Zirlo sample. Figure 39 shows the surface appearance of Gd-alloyed Zirlo and control Zirlo samples after the autoclave tests.

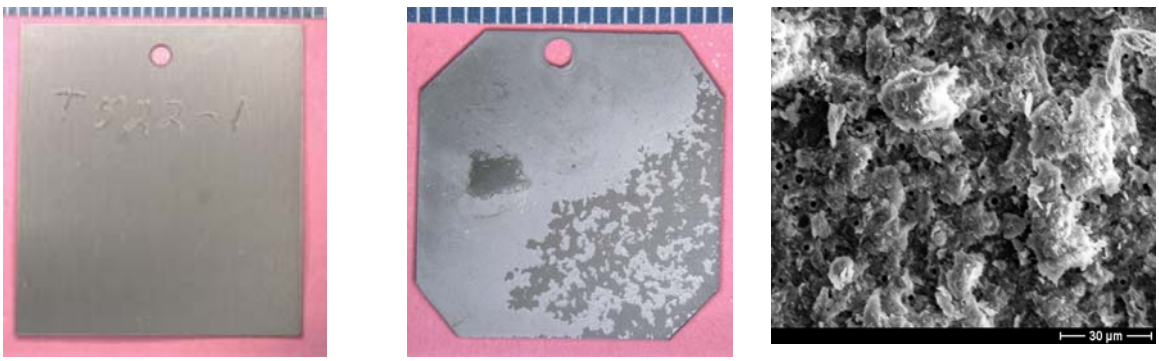

(a) (b) (c)

Figure 39. Oxidation performance of IFBA Gd-alloyed Zirlo in pressurized steam environment at 800°F for 24 hours, (a) control Zirlo, (b) Gd-alloyed Zirlo, and (c) high magnification SEM image of oxidation in Gd-alloyed Zirlo. Gd-alloyed Zirlo exhibited 2 to 3 times greater weight gain due to oxidation compared to the control Zirlo sample.

To arrive at a solution to the oxidation problem a innovative multi-layer sandwich structure approach was investigated, wherein the Gd-alloyed Zirlo layer is topped off with a pure zirconium layer as shown schematically in Figure 40. The result is a 'buried' gadolinium IFBA layer, with an outermost corrosion resistant layer. This multi-functional, multi-layer has the potential to provide oxidation resistance, while at the same time allowing of the synthesis of a Gd-alloyed sub-surface layer.

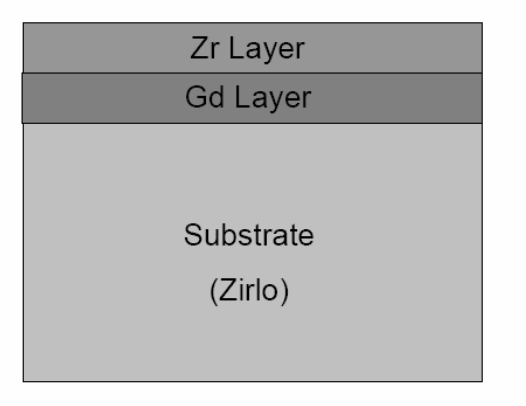

Figure 40. Schematic illustration of the multi-functional, multi-layered surface treatment to create a IFBA Gd-rich sub-surface layer and an outer corrosion resistant Zr layer.

To achieve this objective, three process approaches were investigated using Sandia's IBEST process (Figures 41, 42, and 43).

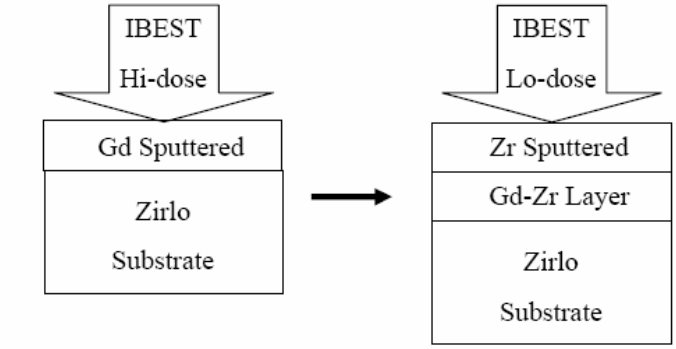

Figure 41 (Approach 1): Sputter deposit a thin layer of Gd followed by high dose IBEST treatment for producing a Gd-Zirlo alloy layer, followed by zirconium sputter deposition, and then use a low-dose IBEST treatment.

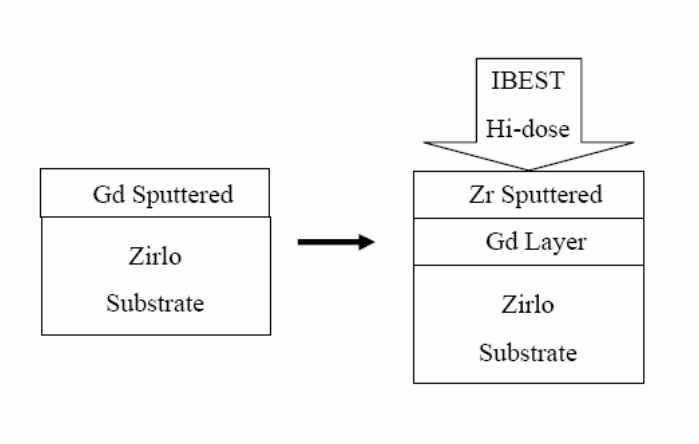

Figure 42 (Approach 2): Sputter a thin film of gadolinium then follow up by sputtering a thin film of zirconium, and then use a single high dose IBEST treatment of the multilayer.

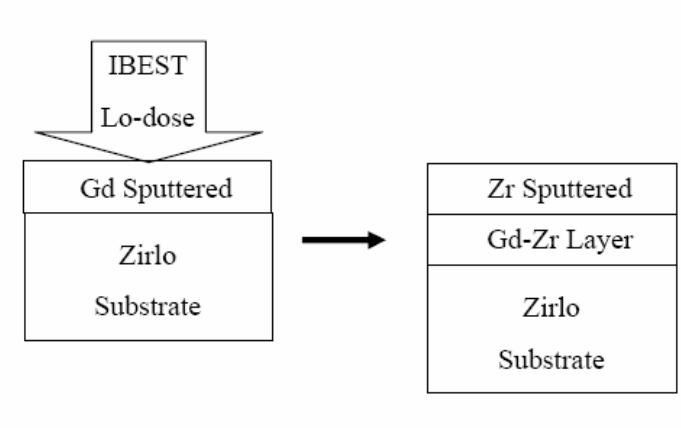

Figure 43 (Approach 3): Sputter deposit a thin layer of gadolinium, treat with low dose IBEST, followed by sputter deposition of an outer zirconium layer.

All three approaches are aimed at one central objective, namely to create a surface multilayer structure on Zirlo alloy consisting of an outermost oxidation resistant Zr layer and a sub-surface Gd layer. Within the framework of this broad objective the three approaches (illustrated in Figures 41, 42, and 43) result in fundamentally different micro- or even nano- structures.

The first approach (Figure 41) uses the most number of processing steps and is perhaps the most aggressive in terms of ion bombardment. It involves high dose alloying of initially sputter deposited Gd layer (the high dose promotes alloying, but at the same time has the negative effect of promoting ablation of the sputtered layer). This is followed by sputter deposition of a zirconium layer which is treated with low dose in order to alloy the surface, but at the same time avoid undue ablation of the Zr layer.

The second approach (Figure 42) involves sequential sputter deposition of Gd and Zr followed by a high dose treatment of the dual sputtered layer. This is expected to create alloying at the interface of the Zr and Gd layers while melting the Zr layer and partially melting the underlying Gd layer.

The third approach (Figure 43) involves Gd sputter deposition followed by low dose treatment to preserve the Gd layer from ablation followed by a final sputter deposition of a Zr

layer. Unlike the first two approaches, the third approach retains a sputtered layer structure at the outer surface.

Our SEM and x-ray diffraction (XRD) analysis work(Figures 44, 45, and 46) showed that all three approaches were successful in achieving the central objective, namely to create a surface multilayer structure on Zirlo alloy consisting of an outermost corrosion resistant Zr layer and a sub-surface Gd layer. To establish this, SEM-EDS analysis was performed using two acceleration voltages, 15KV and 25 KV. Higher accelerating voltages result in greater penetration of the electrons into the sample surface, and the chemical information thus derived comes from greater depths. Conversely, lower accelerating voltages lead to shallow electron penetration into the sample surface and the chemical information in this case comes largely from outer surface layers of the sample, at least in relative terms. Similarly, XRD was performed using conventional x-ray diffraction (CXRD) and grazing incidence x-ray diffraction (GXRD). In CXRD x-rays penetrate substantially deeper than in GXRD, and consequently the phase information in this case comes for the a greater depths into the sample surface. As shown in Figure 44through 46, both SEM (low and high accelerating energies) and x-ray diffraction (CXRD and GXRD) were used to effectively to establish the presence of an outer Zr layer and a buried sub-surface Gd layer for samples produced using all three approaches.

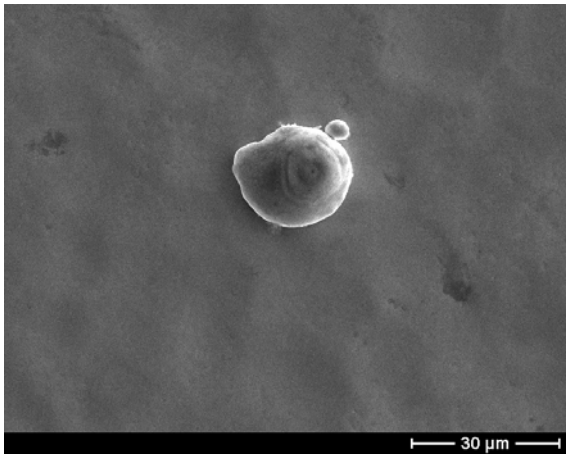

(a)

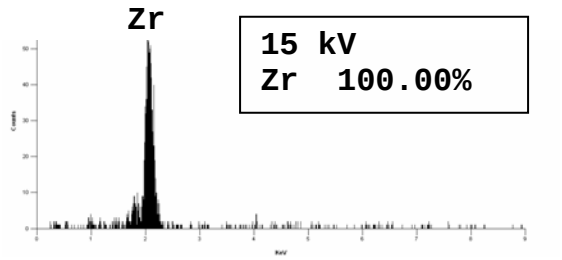

(b)

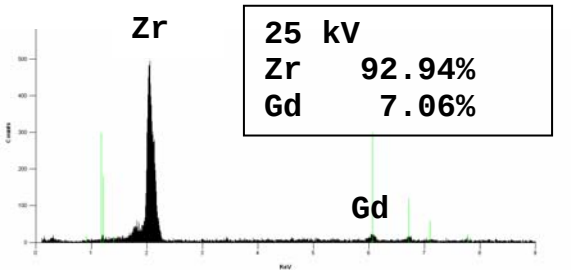

(c)

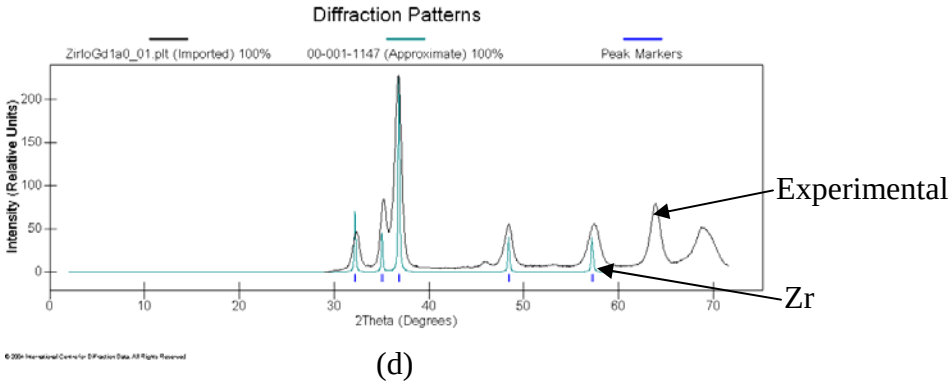

(d)

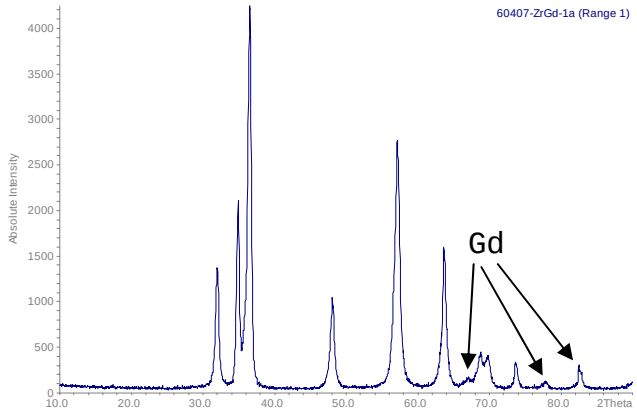

(e)

Figure 44. Approach 1: (a) SEM image of the surface showing a homogeneous surface, (b) SEM-EDS analysis at 15KV showing only the Zr surface layer, (c) SEM-EDS analysis at 25KV showing surface Zr and subsurface Gd, (d) GXRD showing only surface Zr, and (e) CXRD showing surface Zr and subsurface Gd.

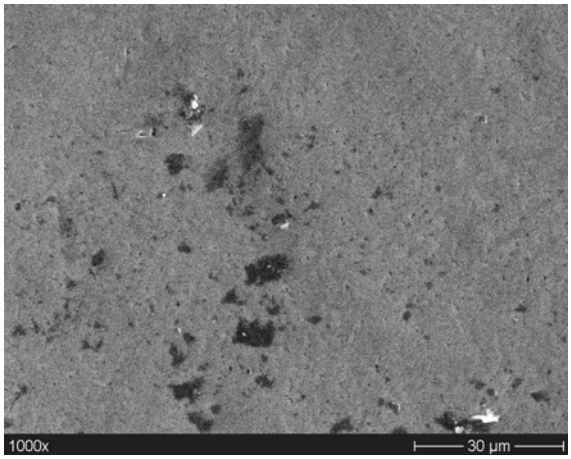

(a)

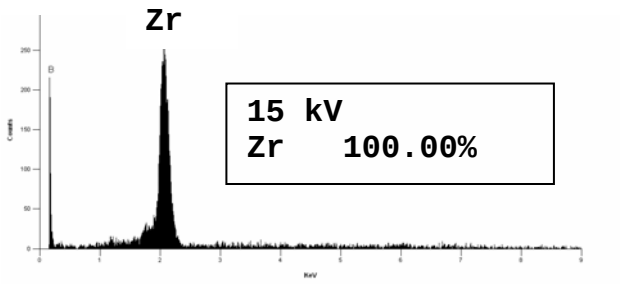

(b)

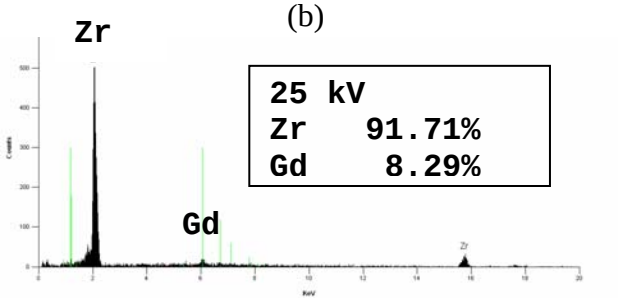

(c)

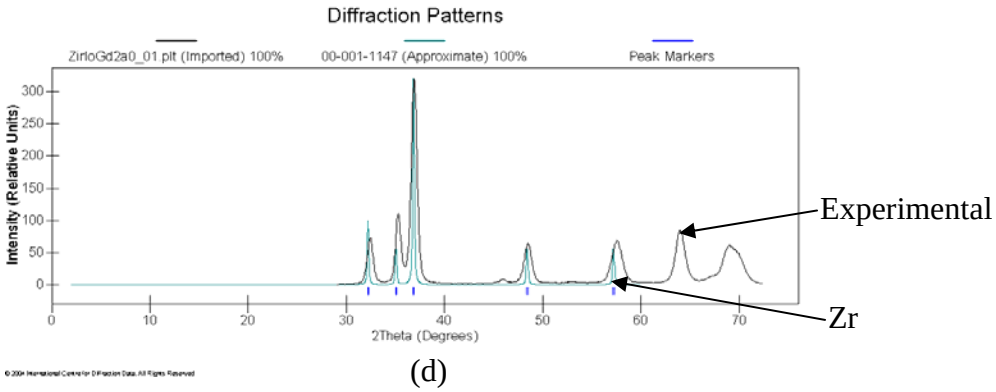

(d)

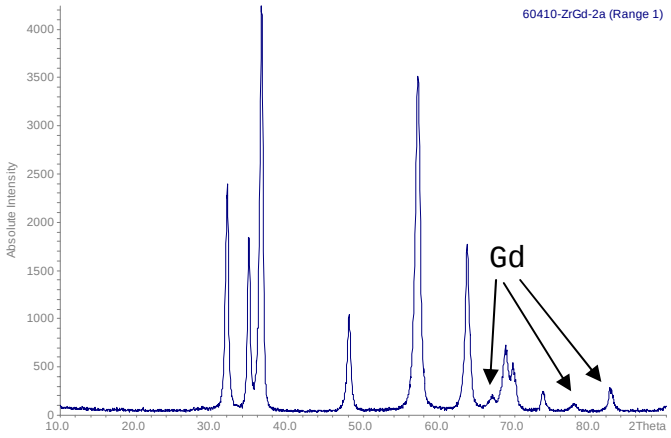

(e)

Figure 45. Approach 2: (a) SEM image of the surface showing a homogeneous surface, (b) SEM-EDS analysis at 15KV showing only the Zr surface layer, (c) SEM-EDS analysis at 25KV showing surface Zr and subsurface Gd, (d) GXRD showing only surface Zr, and (e) CXRD showing surface Zr and subsurface Gd.

(a)

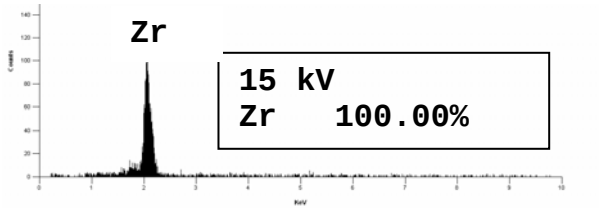

(b)

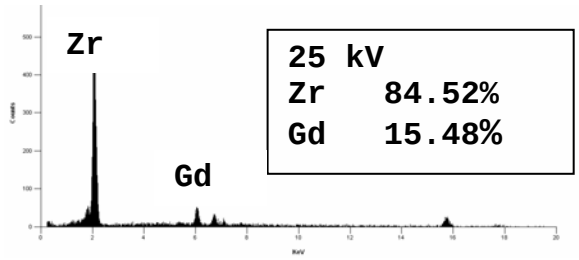

(c)

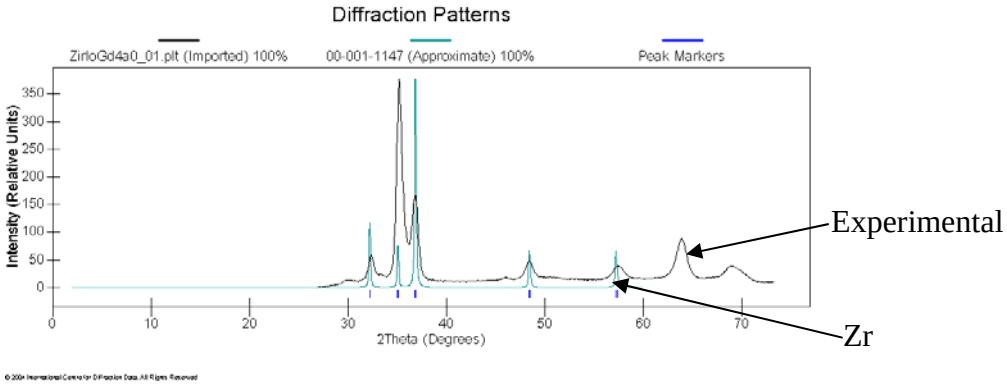

(d)

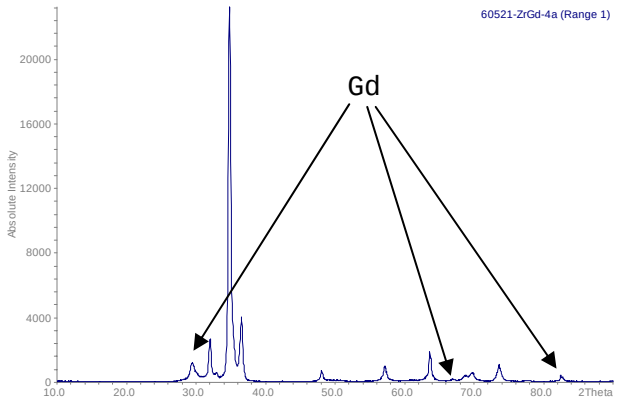

(e)

Figure 46. Approach 3: (a) SEM image of the surface showing a homogeneous surface, (b) SEM-EDS analysis at 15KV showing only the Zr surface layer, (c) SEM-EDS analysis at 25KV showing surface Zr and subsurface Gd, (d) GXRD showing only surface Zr, and (e) CXRD showing surface Zr and subsurface Gd.

Autoclave testing of the multilayered surfaces in high temperature, high pressure steam at Westinghouse did not show promising results.

13. Radiation testing at Idaho National Laboratory

Boron-IBEST surface treated and zirconium diboride cold sprayed Zirlo samples are presently being tested for radiation stability at Idaho National Laboratory's GFR facility. The samples have now been exposed for about 2 years. Since 'hot' radiated samples cannot be evaluated at UW, we have arranged for a graduate student from our group (Mr. Brandon Miller, who is interning at INL) to perform TEM analysis of the samples on-site at INL. Mr. Miller is certified to use the facilities at INL and is in fact conducting his research at INL on electron microscopy of irradiated metal-oxide fuel samples.

14. Presentations: The work was presented by student Mr. Jesse Gudmundson at the University of Wisconsin, Undergraduate Research Symposium in April 2007. The symposium consisted of selected poster sessions from students across the campus. Mr. Gudmundson also presented his work on this research at the DoE-NEER sponsored technical session at the American Nuclear Society Annual Conference in Boston, June 2007. Poster presentation of the work at the ANS Nuclear Fuels and Structural Materials symposium held in conjunction with American Nuclear Society Annual Conference in Anaheim in June 2008. We plan to submit a journal article on this work by the end of this calendar year.

15. Summary and Conclusions: Two surface treatment processes, an ion-based surface engineering process, IBEST and a cold spray process for coating ZrB_2 have been investigated for the incorporation of the IFBA element boron in the surface of fuel cladding materials. The long-term goal of this research concept is to incorporate boron in the outer surface of fuel cladding as an alternative to their addition to the fuel pellets. From a materials science standpoint both approaches successfully achieve this objective, as demonstrated on Zirlo, NF616 ferritic steels, and 316 austenitic stainless steel fuel cladding materials. Using the non-equilibrium IBEST process, substantial amounts of boron (~ 25 at%) were alloyed up to depths of 3 to 4μm, even though boron is largely insoluble in these materials. The cold spray process resulted in a well-adhered coating (1 to 2μm thick) of ZrB_2 on the surface, with evidence of a metallurgical bond between the coating and the substrate. Testing in supercritical water at 500^{o}C and steam at 427^{o}C, showed these surface treated layers to be quite stable in these high temperature environments, up to exposure durations of 165 hours. The corrosion resistance of Zirlo and NF616 ferritic steel were not significantly altered as a result of these surface treatments in either the supercritical water or steam environments. There was a slight decrease in the corrosion resistance of 316 austenitic stainless steel. Overall, these high temperature tests demonstrated that the IFBA boron can be incorporated at the surface of fuel cladding without adversely affecting their corrosion resistance. Of the two surface treatments, IBEST at present is a more research-oriented process with considerable potential for research in basic materials science. The process is performed in vacuum and being line-of-sight, it may be expensive to build and operate a commercial system that can treat surfaces of large numbers of full-length fuel claddings. The cold spray process on the other hand is very commercially feasible, both technically and economically and holds considerable promise for the surface treatment of outer surfaces of fuel claddings with IFBA element boron.

DEPARTMENT OF ENERGY MANDATED DISCLAIMER

"This report was prepared as an account of work sponsored by an agency of the United States Government. Neither the United States Government nor any agency thereof, nor any of their employees, makes any warranty, express or implied, or assumes any legal liability of responsibility for the accuracy, completeness, or usefulness of any information, apparatus, product, or process disclosed, or represents that its use would not infringe privately owned rights. Reference herein to any specific commercial product, process, or service by trade name, trademark, manufacturer, or otherwise does not necessarily constitute or imply its endorsement, recommendation, or favoring by the United States Government or any agency thereof. The views and opinions of authors expressed herein do not necessarily state or reflect those of the United States Government or any agency thereof."